



# Synthesis of high-modulus thermoset PUs of PCL-PTMG/CNW biomaterials with different soft domain architecture and composition for high shape memory performance

Elahe Aboueimehrizi · Mohammad Amin Makaremy · Sina Bazrpash · Fatemeh Noormohammadi · Yasaman Rahimi Darestani · Mohammad Nourany

Received: 10 March 2022 / Accepted: 9 August 2022 / Published online: 17 August 2022  
© The Author(s), under exclusive licence to Springer Nature B.V. 2022

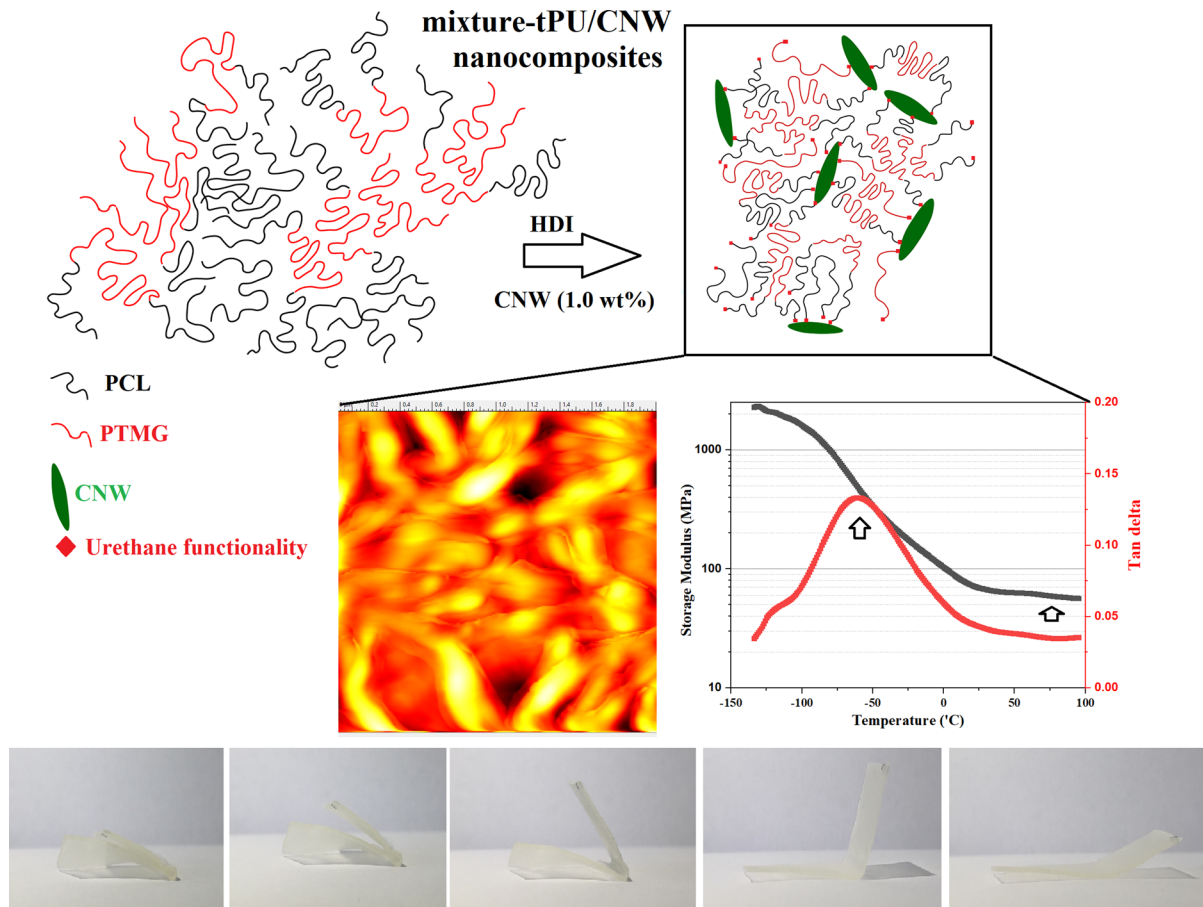
**Abstract** In this research work, a series of thermoset polyurethane (tPU) nanocomposites and a thermoplastic PU (TPPU) were synthesized using semi-crystalline polyols. Poly( $\epsilon$ -caprolactone) (PCL), poly(tetramethylene glycol) (PTMG), and different architecture and compositions of PCL and PTMG were used as diols. PCL was used to synthesize a TPPU (PCL-TPPU) as the control specimen. Cellulose nanowhisker (CNW), with 1.0 wt% content, was used for synthesis of the tPU nanocomposites. The aim of this research was to investigate the impact of the thermosetting using CNWs and tuning crystallization of the polyols on the shape memory performance

(SMP) of PUs. The analysis of the polyols' crystallization and crystallization of the soft segments in the PU structures was studied to evaluate the impact of structural changes on the SMP of the PUs. The results of the dynamic mechanical thermal analysis showed that the tPUs have a large elastic modulus ( $E'$ ) at temperatures around  $\sim 25$ – $40$  °C ( $\sim 10$  MPa) and very small  $\tan\delta$  height (below 0.15), which was attributed to their thermoset nature and presence of CNW with high  $E'$  value ( $\sim 110$ – $220$  GPa). The PCL-TPPU, as the control specimen, showed  $E'$  in the range of 200–400 kPa. The PUs have also proved to be highly biocompatible.

---

E. Aboueimehrizi · M. A. Makaremy · S. Bazrpash · F. Noormohammadi · Y. R. Darestani · M. Nourany (✉)  
Polymer Engineering and Color Technology, Amirkabir University of Technology, Tehran, Iran  
e-mail: m.nourany@aut.ac.ir

## Graphical abstract



**Keywords** Cellulose nanowhisker · Thermoset polyurethane · Thermomechanical properties · Shape memory performance

## Introduction

Thermoplastic polyurethanes (TPPUs) and thermoset polyurethanes (tPUs) are a family of polymers that possess inherent thermal shape memory performance (SMP) (Jiu et al. 2016; Joo et al. 2018; Shirole et al. 2018). They can be thermally programmed through different heating and cooling cycles to undergo a reversible shape switching process between a permanent shape ( $L_1$ ) and a strain-induced temporary shape ( $L_2$ ). In a thermally programmable polymer there

exists two main characteristic temperatures: switching temperature ( $T_s$ ) and recovery temperature ( $T_r$ ); and there exists two structural components: switching component (SC) and permanent component (PC) (Joo et al. 2018; Wang et al. 2018b; Kausar 2019). In a TPPU system, the hard domains play the role of the PC. In TPUs, the physical cross-link nature of the hard domains prohibits the slippage of the SC chains (Cao and Jana 2007; Wang et al. 2018a; Urbina et al. 2019). For TPPUs, the curing condition, including time and temperature, and the nature of hard segments would impact the ability of the hard segments to form segregated domains, which consequently impacts their SMP (Choi et al. 2012; Kausar 2019). However, for a tPU, the possibility of hard segment–soft segment mixing is eliminated and the

final shape recovery improves to a large degree (Jiu et al. 2016). In a tPU structure, the soft domain plays the role of SC, and the cross-link points act as the PC (Jafari et al. 2020; Noormohammadi et al. 2021; Ranjbar et al. 2021). The SMP of PUs is defined by their ability to fix a temporary shape (shape fixity) and the ability to recover the original shape (shape recovery) (Jafari et al. 2020). It is known that elastic modulus plays a key role in tuning SMP. Thermosetting and the use of high modulus nanoparticles are two main procedures to improve elastic modulus (Ranjbar et al. 2021). In recent years, cellulose nanowhisker (CNW) has been the focus of numerous researches (Lu and Hsieh 2010) as the CNW is considered as a highly elastic nanorod particle, with an elastic modulus in the range of  $\approx 110$ – $220$  GPa. Upon ideal dispersion in polymer matrices, they can act as an efficient mediator to transfer the external applied energy in the direction of applied force and also increase the elastic modulus of the composites (Lahiji et al. 2010; Domingues et al. 2014; Tang et al. 2017).

CNWs are extracted from natural resources including cotton, wood, rice straw, and other cellulose-rich plants (George and Sabapathi 2015; Roman et al. 2009). Different extraction procedures were developed to isolate CNWs from their raw materials including acid-hydrolysis, oxidization method, ionic liquid and enzymatic hydrolysis (Trache et al. 2017; Vanderfleet and Cranston 2021). Each of these four main procedures have their own advantages and disadvantages. However, regarding the cost and time of the extraction process, acid-hydrolysis was considered as the main choice available for efficient extraction (Mariano et al. 2014). Cotton was also considered as the main renewable resource of CNWs (Xie et al. 2018; Du et al. 2019). The CNWs isolated from cotton by acid-hydrolysis had a crystallinity of 79–83% (SaifulAzry et al. 2021), an yield in the range of 57–69% with a diameter and length of 9–19 nm and 157–290 nm, respectively (Reid et al. 2017; Mu et al. 2019). CNWs have abundant -OH groups, which can be used for further chemical or physical modification (Roman et al. 2009; Tingaut et al. 2012). According to the literature, nanocomposites of thermoplastic polyurethanes (TPPUs) and CNWs have shown an improvement in mechanical properties including Young's modulus (Rueda et al. 2013; Fortunati et al. 2017; Prataviera et al. 2018). Despite substantial research in this field, application

of CNWs as an active agent in the field of thermoset polymers is limited (Pei et al. 2021). Their role as a cross-linking agent and their impact on the thermo-mechanical properties of the final thermoset polymer nanocomposites has not been fully investigated (Park et al. 2013).

In this work, different microstructures of polyols were prepared using PCL and poly(tetramethylene glycol) (PTMG). The polyols were composed of neat PCL and PTMG, with molecular weights of 2000 g/mol, their 50:50 w:w blends, the tri-block of PCL<sub>1000</sub>-PTMG<sub>2000</sub>-PCL<sub>1000</sub> and the 100:50 w:w ratio of the blend and the block copolymer. Their crystallization behavior was studied. These specimens were further used to prepare thermoset PU/CNW nanocomposites. A thermoplastic PU of PCL (Mw: 2000 D) (PCL-TPPU) was synthesized as the control specimen to compare the different between the thermoplastic and thermoset PUs. The crystallization and dynamic behavior of the synthesized PUs were also studied. The mechanical properties, the shape memory performance of the PUs and the impact of the change in elastic modulus on shape fixity and recovery was thoroughly investigated. The cytocompatibility of the PUs was studied to evaluate their potential for biomedical applications.

## Experimental section

### Materials

Poly( $\epsilon$ -caprolactone) with molecular weight of 2000 D (PCL<sub>2000</sub>), Hexamethylene diisocyanate (HDI), Stannous Octoate (Sn(Oct)<sub>2</sub>), Dibutyl tindilaurate, and butane-diol (BDO) were purchased from Sigma and were used as received. Dimethylformamide (DMF, Sigma), Sulfuric acid (98%, sigma) were also used as received. Refined cotton (Iran, Golestan) was used as the source for extraction of cellulose nanocrystals. Poly(tetramethylene glycol)-diol (Mitsubishi chemical co.) with a molecular weight (Mw) of 2000 D (PTMG<sub>2000</sub>). DMEM and FBS (Gibco, UK), and penicillin/ streptomycin (Sigma). Culture plates and flasks (United Scientific F1004 Plastic Well Plate).

## CNW extraction

The CNW extraction from purified cotton is fully described in our previous work (Noormohammadi et al. 2021). Here, we describe the procedure in brief. The sulfuric acid (98%) hydrolysis procedure was used for hydrolysis of cotton. 5 gr cotton and 100 mL acid solution in distilled water with a relative acid to water content of 50 mL: 50 mL was used for the hydrolysis procedure. The final suspension was centrifuged at 5000 rpm to extract the CNWs. Dialysis tube was used for increasing the pH of the CNWs to a range of 6.5–7.0. The surface-charge neutralized CNWs were further freeze-dried.

## Block copolymer synthesis

The PCL<sub>1000</sub>-PTMG<sub>2000</sub>-PCL<sub>1000</sub> block copolymer (Block 1:1) was synthesized using a pseudo-anionic bulk polymerization at 120 °C. Stannous Octoate (Sn(Oct)<sub>2</sub>) with a ratio of 0.2 mol% relative to PTMG<sub>2000</sub> was used as the catalyst. In the first step of the polymerization, 10 gr of PTMG with a molecular weight of 2000 D was added to a 50 ml round bottom 3-neck flask and heated to 120 °C. Then, vacuum was applied to the melt to remove moisture and possible contamination. Sn(Oct)<sub>2</sub> was added to the flask.  $\epsilon$ -caprolactone monomer (5.3 ml) was added to the flask and the flask was then sealed and the reaction was kept to proceed for 24 h. The termination phase was performed using 5 ml solution of distilled water and a few droplets of 37% HCl. The final copolymer was precipitated in cold ether solvent. The efficiency of the polymerization was 94.6% and the resulted of Gel Permeation Chromatography showed that the final block copolymer possessed a number-averaged molecular weight of 4127 D with a PDI of 1.22.

## Thermoset polyurethane synthesis

Table 1 provides the formulation recipe for synthesis of the thermoplastic PU and the thermoset PU/CNW nanocomposites. The molar ratio of HDI to each polyol was kept at 3:1. For synthesis of the control specimen of thermoplastic PU, BDO was used and for the thermoset PU nanocomposites the CNW content was 1.0 wt% relative to the prepolymer.

The synthesis procedure is as follows: (1) Weighting the polyol(s) and adding them into the 3-necked bottom round flask; (2) heating and stirring the polyol(s) at 80 °C and 250 rpm; (3) using vacuum for 15 min to eliminate the possible moisture and then, applying a continuous dry nitrogen purge; (4) adding the PU catalysis solution, Dibutyl tin dilaurate in DMF, to the polyol(s) using a syringe; (5) dropwise addition of HDI to the reaction media and allowing the reaction to proceed for 2 h to ensure complete conversion of diols into prepolymers; (6) adding BDO or the pre-sonicated CNW in DMF suspension to the flask; (7) allowing for the reaction to proceed for 30 min and then pouring the highly viscose solution into Teflon mold; finally, (8) putting the Teflon mold in oven at 70 °C for 24 h. For synthesis of the PCL-based thermoplastic PU (PCL-TPPU), the molar ratio of PCL:HDI:BDO was set to 1:3:2.

## Cross-link density and degree measurement

The equilibrium swelling test was used for measuring the cross-link density (CLD) of the thermoset PU/CNW nanocomposites. Three samples of each specimen with dimensions of 1 cm × 1 cm × 1 mm were cut and then immersed into a glass containing toluene and the result for each specimen was averaged over three. The samples were kept in the solvent for 72 h at room conditions. The sealed glass containers were placed on a shaker to ensure dissolution of unreacted

**Table 1** The formulation recipe for synthesis of the thermoset PU synthesis

Specimen	PCL <sub>2000</sub> (gr)	PTMG <sub>2000</sub> (gr)	Block 1:1 (gr)	HDI (gr)	BDO (gr)	CNW (gr)
PCL-TPPU	12	0	0	3.02	1.08	0
PCL-tPU	12	0	0	3.02	0	0.150
PTMG-tPU	0	12	0	3.02	0	0.150
Block 1:1-tPU	0	0	12	1.51	0	0.135
Blend-tPU	6	6	0	3.02	0	0.150
Mixture-tPU	4	4	4	2.52	0	0.145

polyols into the solvent. The final stable weight of the swollen samples was selected as the equilibrium swelling weight (ESW). The thermodynamically developed Flory–Rehner equation, Eq. 1, was applied to measure the CLD.

$$v = \frac{-[\ln(1 - V_r) + V_r + \chi V_r^2]}{V_0 \left( V_r^{\frac{1}{3}} - 0.5V_r \right)}, \quad (1)$$

The parameters of  $v$ ,  $V_0$ ,  $\chi$ , and  $V_r$  represent the CLD, solvent molar-volume, polymer–solvent interaction parameter, volume fraction of the swollen thermoset PU/CNW nanocomposite. The cross-link degree or gel content of the specimens is measured using a Soxhlet extractor. Again, three samples of each specimen with dimensions of 1 cm × 1 cm × 1 mm were cut and placed into the Soxhlet and Toluene was used as the solvent. The siphon tube would create a flow to remove the dissolved polyols and procedure proceeded for 24 h. The final dry-weight of the specimens was measured and divided by the original weight to get the gel fraction.

#### Shape memory procedure

The shape memory performance analysis of the thermoset PU specimens was performed through two different procedures. In the first procedure, the specimens with 2.5 × 1 × 0.1 cm<sup>3</sup> dimensions were bend over and fixed using a metal clamp. Then, the specimens were immediately put into liquid nitrogen for 5 min. Allowing for more freezing process time leads to brittleness and fracture of the specimens. In the next step, the specimens were put at room temperature and the clamp was removed. The camera was set to take pictures of the specimens every 15 s to follow the shape recovery process. The second procedure was to use a DMA instrument working in tension mode. The specimens' dimension was 2 × 0.5 × 0.1 cm<sup>3</sup>. The thermal programming procedure was as follows: (A) increasing temperature to 37.5 °C; (B) applying a 30 N dynamic force to stretch the specimens; (C) decreasing temperature to − 25 °C; (D) Removing the force; (E) Increasing the temperature to 37.5 °C. The parameters of the shape memory performance, recovery ratio ( $R_r$ ) and fixity ratio ( $R_f$ ), are defined as Eqs. 2 and 3, respectively.

$$R_r = \frac{L_1 - L_3}{L_1}, \quad (2)$$

$$R_f = \frac{L_2}{L_1}; \quad (3)$$

$L_1$ ,  $L_2$  and  $L_3$  represent the stretched length at the elevated temperature, the length after unloading the applied force and the specimen length at the end of the recovery process.

#### Cell culture procedure

The Human Foreskin Fibroblast (HFF) cells were seeded onto the thermoset PU/CNW nanocomposites according to the procedure described in detail in our previous paper (Jafari et al. 2020). Here, we describe the procedure in summary: (1) washing the PU films with distilled water and after drying, they were UV-sterilized; (2) Tissue-culture grade polystyrene (TCPS, 48 wells) was used for cell seeding onto the tPU/CNW nanocomposite films; (3) HFF cells suspended in DMEM, with 10% FBS and 1% penicillin/ streptomycin, with a cell density of 2 × 10<sup>4</sup> cells/specimen were seeded on the tPUs; (4) Using the standard condition of 37 °C with 96% humidity and 5% CO<sub>2</sub> atmosphere in the incubator for maintaining the seeded cells; (5) The cell fixing was performed by 2.5% glutaraldehyde. The cell viability of the HFF cells seeded onto the tPU/CNW nanocomposites was measured through MTT assay. After 3 and 5 days of culture, 50 ml of MTT solution (5 mg/ml) was added to each one of the wells. The plates then were incubated for three hours. At the end, the supernatant was collected and a micro-plate reader (BioTek) was used for analysis of optical density. The cell viability is measured using Eq. 4.

$$\text{Cell Viability (\%)} = \frac{OD}{OD_0} \times 100 \quad (4)$$

OD and OD<sub>0</sub> represent the optical density of suspensions related to cell-seeded plates and the blank control, respectively.

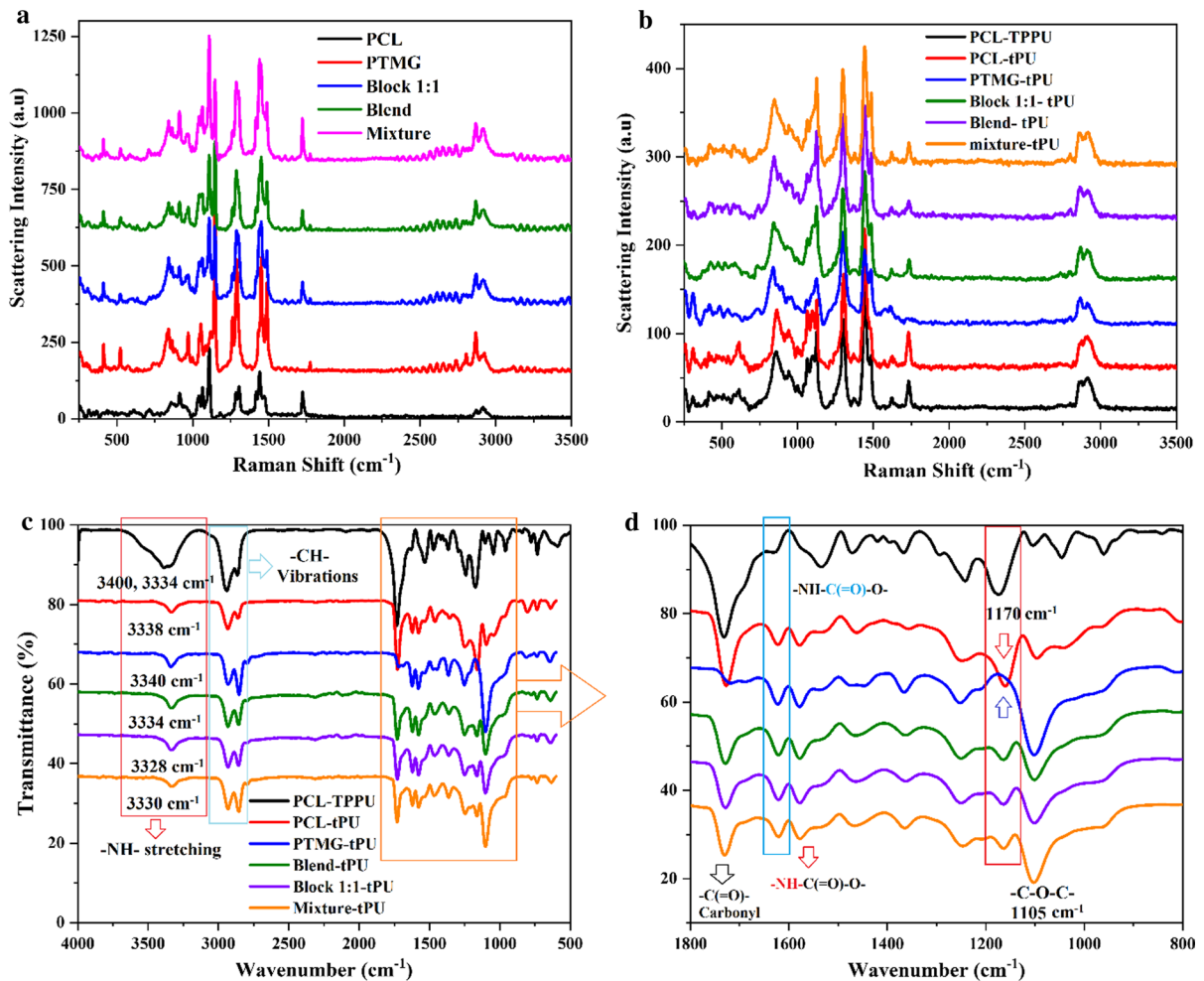


**Fig. 1** Raman spectroscopy of **a** the polyols and **b** the thermoset PU nanocomposites. **c, d** ATR-FTIR spectrum of the synthesized thermoset PU nanocomposites

## Characterization

The chemical structure analysis was performed using ATR-FTIR (MOD SRG 1100G, BOMEM) and Raman spectroscopy (Confocal Raman Microscope, equipped with two laser wavelengths of 532 and 785 nm). Scanning electron microscopy (SEM), Phenom Pharos, used for surface and cross-section imaging. Dynamic mechanical analysis (DMA, Triton, TA) was performed for phase behavior and shape memory performance analyses. Differential scanning calorimetry (DSC, Mettler/Toledo) was used for

analysis of crystallization with a heating and cooling rate of 10 °C/min. The stress–strain analysis was performed using the tensile instrument (BONGSHIN, model: DBBP-2 t) with a jaw speed of 20 mm/min. The surface topography of the thermoset PU/CNW nanocomposites was analyzed using AFM (NT-MDT co.) instrument operating at room temperature in tapping mode. Inverted fluorescent microscopy was used to analyze the state of the seeded HFF cells after three and five days. For this analysis, the cells were fixed and treated with DAPI for cell staining.

## Results and discussion

### Raman spectroscopy

According to Fig. 1a, the characteristic Raman bands of crystalline and amorphous PCL segments are summarized as follow:  $917\text{ cm}^{-1}$  ( $\nu\text{-C-C (}=\text{O)-O-}$ ) crystalline,  $1030\text{--}1120\text{ cm}^{-1}$  (skeletal stretching,  $1071\text{ cm}^{-1}$   $\nu\text{-C-O-C}$ -crystalline),  $1276\text{--}1352\text{ cm}^{-1}$  ( $\omega\text{ CH}_2$ ),  $1410\text{--}1487\text{ cm}^{-1}$  ( $\delta\text{ CH}_2$ , 1445 crystalline),  $2835\text{--}3000\text{ cm}^{-1}$  ( $\nu\text{ CH}$ , crystalline)(Parnell et al. 2003); regarding PTMG, the Raman bands are as follow:  $2939$ ,  $2887$ ,  $2840\text{ cm}^{-1}$  (alkyl chains),  $1478$ ,  $1442\text{ cm}^{-1}$  (bending mode of C-H group),  $1278$ ,  $1226\text{ cm}^{-1}$  (CH twisting vibrations),  $1123\text{--}1146\text{ cm}^{-1}$  (C-O, C-OH, C-C),  $846$ ,  $860\text{ cm}^{-1}$  (skeletal vibrations), and  $533$ ,  $362\text{ cm}^{-1}$  C-O-C bending (Tian et al. 2019; Wu et al. 2021). The Raman spectrum of the blend, block copolymer and their mixture indicate presence of both PCL and PTMG segments.

Figure 1b shows the Raman spectrum of the synthesized PCL-TPPU and the thermoset PU/CNW nanocomposites. The characteristic isocyanate bands, which are  $\text{-N=C=O}$  asymmetric stretching band at  $2272\text{ cm}^{-1}$  and symmetric stretching at  $1443\text{ cm}^{-1}$  are absent in the spectrum as an indication of complete consumption of the functionality. Based on the images, the polyurethane bands are as follows:  $\text{-NH-}$  (amide I  $1732\text{ cm}^{-1}$ , amide II  $1530\text{ cm}^{-1}$ , amide III  $1303\text{ cm}^{-1}$ ), Ester  $\nu(\text{C=O})$  (urethane amide I  $\nu(\text{C=O})$   $1732\text{ cm}^{-1}$ ,  $\delta(\text{CH}_2)$ :  $1443\text{ cm}^{-1}$  and  $\delta(\text{CH})$  (urethane amide III  $1249$ ) (Ha et al. 2019; Qu et al. 2021). The band related to the ester carbonyl group is not available in the Raman spectrum of the PTMG-tPU and its intensity for the other three tPU specimens is lower than that of PCL-tPU.

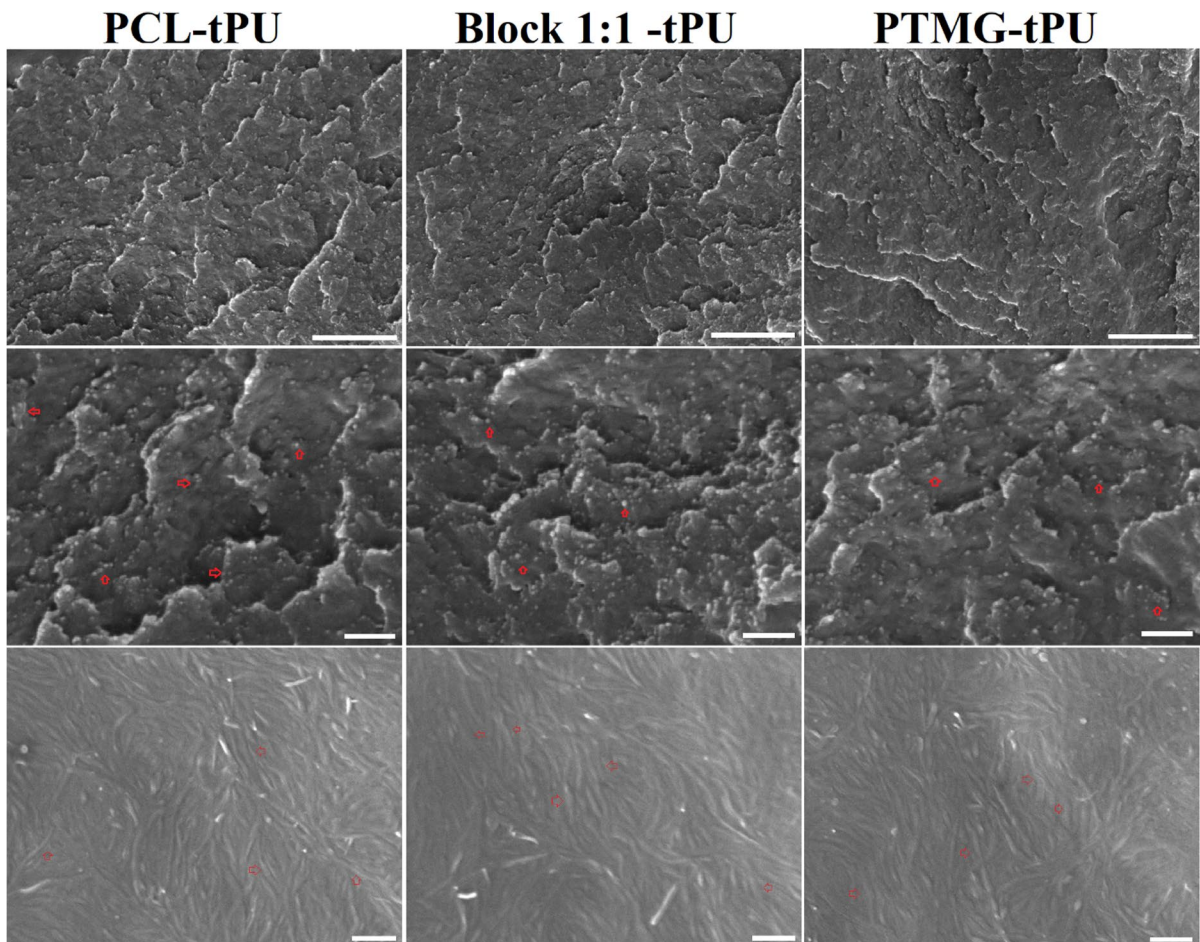
### FTIR analysis

Figure 1c represents the full FTIR spectrum of the synthesized PUs. The absorption peaks in the wave-number range of  $900\text{--}1800\text{ cm}^{-1}$ , which is represented in Fig. 1d, provides the majority of the structural information on the soft segments and the urethane functionality. Based on Fig. 1c, the absorption peak around  $3332\text{ cm}^{-1}$  corresponds to the stretching vibrations of  $\text{-NH-}$  groups in the urethane group formed by the condensation reaction between the  $\text{-N=C=O}$  group in the prepolymers' structure

and the  $\text{-CH}_2\text{-OH}$  groups available on the CNW surface. The  $\text{-NH-}$  group in the urethane group usually shows two absorption peaks at  $3330$  and  $3340\text{ cm}^{-1}$ , which are related to hydrogen-bonded and free  $\text{-NH-}$  groups, which is seen in the spectrum of the PCL-TPPU specimen. The single absorption peak at around  $3332\text{ cm}^{-1}$  is due to the lack of free  $\text{-NH-}$  vibrations (Goodarzi et al. 2020), which is specific of thermoset PU nanocomposites (Behrouz et al. 2022). The double peak available in the range of  $2800\text{--}3000\text{ cm}^{-1}$  corresponds to the stretching vibrations of  $\text{-CH-}$  groups in the organic polymer structure. Absence of the peak at  $2200\text{ cm}^{-1}$  for all the specimens indicates that the  $\text{-N=C=O}$  reaction conversion has been completed (Noormohammadi et al. 2021). Regarding the highlighted region, Fig. 1d, the PTMG<sub>20000</sub> polyol is distinguished from PCL<sub>2000</sub> and other soft segments by the absence of the carbonyl ( $\text{-C(=O)-}$ ) peak at  $1734\text{ cm}^{-1}$  (Sarkhosh et al. 2021). The carbonyl peak in the range of  $1700\text{--}1750\text{ cm}^{-1}$  is characteristic of crystalline or amorphous polyesters. Moving towards lower wavenumbers, the two peaks available at  $1624\text{ cm}^{-1}$  and  $1575\text{ cm}^{-1}$  correspond to the stretching vibrations of  $\text{-C(=O)-}$  and bending vibrations of  $\text{-NH-}$  functionalities in the urethane structure ( $\text{-NH-C(=O)-}$ ), respectively (Jafari et al. 2020). The intense peak at  $1105\text{ cm}^{-1}$  available for all the specimens corresponds to stretching vibrations of alkoxy group (Goodarzi and Rao 2021). The peak at  $1170\text{ cm}^{-1}$ , which is present only for polyols with PCL segments, is specific of ester functionalities (Nourany et al. 2021).

### Morphological analysis

Figure 2 shows the SEM cross-sectional and surface images of PCL-tPU, Block 1:1-tPU and PTMG-tPU nanocomposites of CNW. The first and second row images show the cross-sectional images of the cryo-fractured specimens. Based on these images, the CNW nanoparticles with 1.0 wt% content are uniformly distributed and dispersed and there is not any sign of clustering even at  $5\text{ }\mu\text{m}$  scale. The reason for absence of any CNW aggregation or clustering is the covalent attachment of the nanoparticles to the matrix chains (Jafari et al. 2020; Noormohammadi et al. 2021). The third row shows the SEM surface images of the specimens with  $1\text{ }\mu\text{m}$  scale. The images show that the CNWs are aligned on the surface, parallel



**Fig. 2** SEM images of PCL-tPU, Block 1:1-tPU, PTMG-tPU: (first row) cross-section images with 5  $\mu\text{m}$  scale, (second row) cross-section images with 1  $\mu\text{m}$  scale and (third row) surface images of the tPUs with 1  $\mu\text{m}$  scale-bar

to the normal line of the cross-sectional surface, and they seem to have integrated to the matrix.

#### DMTA analysis

The viscoelastic properties of thermoset PUs can be evaluated by DMTA instrument. The results of this test provides insights into the changes in the microstructure of the specimens and the results consist of storage ( $E'$ ) and loss ( $E''$ ) modulus. The ratio of  $E''$  and  $E'$  is called  $\tan\delta$ , which is used to identify the second order transitions (Nourany et al. 2021). In a common  $\log E'$  vs. temperature, there are three main regions and two transitions. The regions are glassy, rubbery plateau and melt states. The two main transitions are glass transition temperature ( $T_g$ ) and flow

(or melting) temperature, which are second and first order transitions, respectively (Sarkhosh et al. 2021). For thermoset polymers, the flow of the specimens are absent and for a semi-crystalline polyol, the melting process of the crystallites can be identified as a one-order of magnitude fall in the storage modulus (Ranjbar et al. 2021). The PUs with linear morphology, also called thermoplastic polyurethanes, show another second order transition for the hard segments in a higher temperature range compared to the soft segments (Jafari et al. 2020). Based on Fig. 3a, it can be seen that the transition for the hard segments is available at 39  $^{\circ}\text{C}$  for the thermoplastic PCL (PCL-TPPU) with peak span of 10–93  $^{\circ}\text{C}$ . However, this transition peak is absent for the tPUs as they are immobilized through covalent bonding to the CNWs



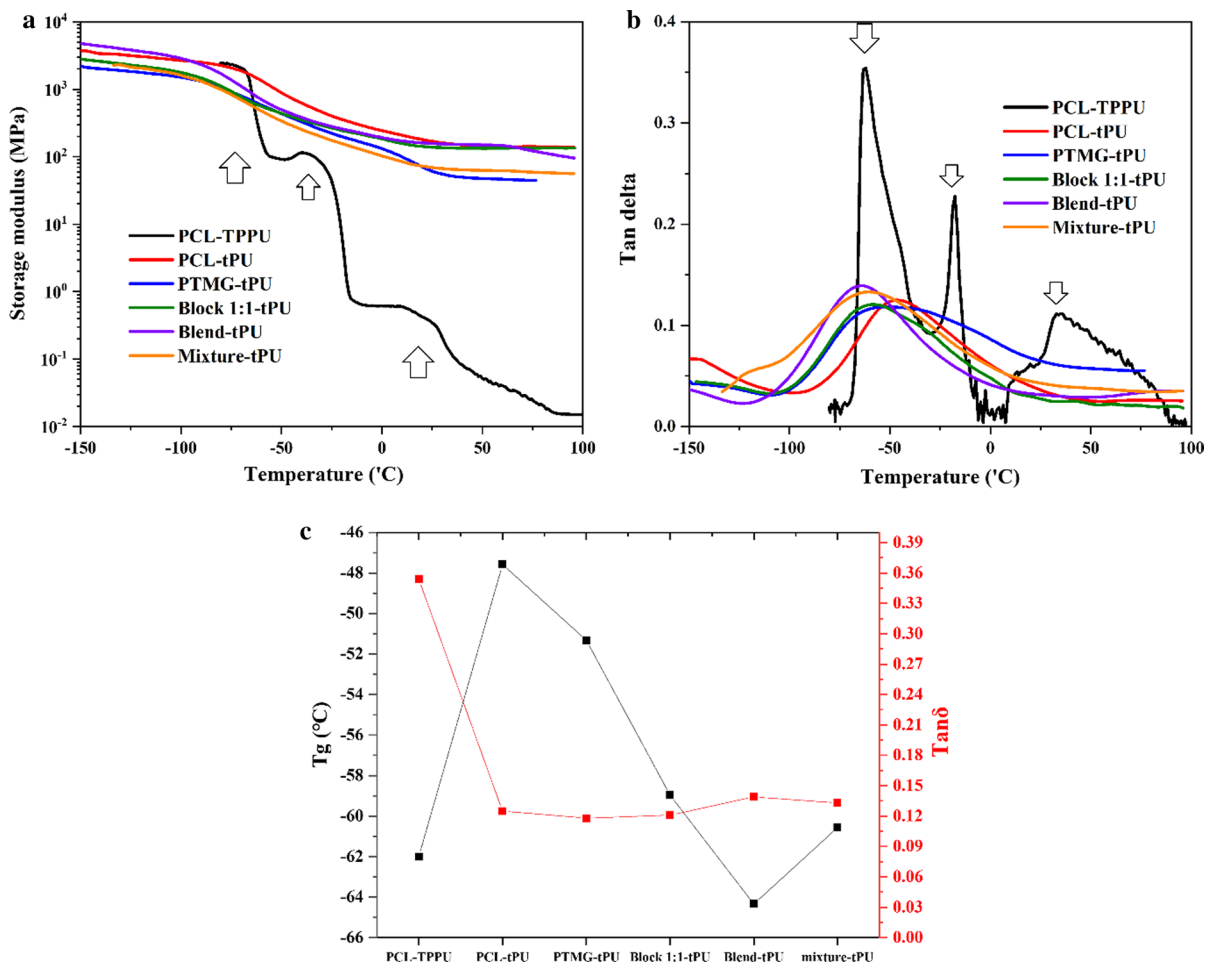


**Fig. 3** a Storage modulus and b  $\tan\delta$  vs. temperature of the synthesized tPUs; c  $T_g$  and  $\tan\delta$  values of the tPUs

and cannot go through a long-range segmental movement. Lack of an upturn in  $\tan\delta$  curves in the temperature range of 50–80 °C, Fig. 3b, confirms absence of this transition (Noormohammadi et al. 2021). As it can be seen from Fig. 3a, the  $T_g$  transition of the soft domain segments of all the thermoset specimens are very broad and extends from – 85 °C to + 15 °C. This feature is specific of semi-crystalline soft segments while amorphous soft segments show an abrupt fall in this region. This feature has also manifested itself in the wide temperature range of  $\tan\delta$  peak for this transition. Amorphous soft segments usually have a  $\tan\delta$  peak height of about 0.5 or higher with a relatively narrow width (Jafari et al. 2020). The PCL-TPPU specimen show a relatively narrower  $\tan\delta$  transition in with a  $T_g$  of – 62 °C and the  $\tan\delta$  peak height is

0.36, which is very higher than the thermoset PU specimens. The reasons for the increased  $\tan\delta$  peak height are the amorphous nature of PCL<sub>2000</sub> polyol, as seen by abrupt fall in storage modulus in this region, and absence of CNWs for this specimen. However, the thermoset specimens possess a very low peak height (below 0.14) confirming their semi-crystalline nature. The  $\tan\delta$  peak heights of each PU specimen is shown in Fig. 3c alongside their  $T_g$ .

Regarding the storage modulus ( $E'$ ) of the thermoset specimens, which is critical in determining the shape memory parameters, it remains high and constant at elevated temperatures. This is due to the thermoset nature of the PU nanocomposites. However, for the PCL-TPPU specimen,  $E'$  experiences multiple abrupt fall and its value falls in the range

of 400–200 kPa for the temperature range of  $-23$  to  $25$  °C. Presence of a second fall in the  $E'$  of PCL-TPPU specimen at  $-16$  °C is related to the phase miscibility of hard/soft segments, which is confirmed by presence of a  $\tan\delta$  peak at this temperature. A high  $E'$ , well above 10 MPa even at  $100$  °C, creates a large driving force for shape recovery process (Zhang et al. 2019a). Another distinct feature of the PU/CNW thermosets is the strong temperature dependency of  $E'$  in the temperature range of  $-85$  to  $+15$  °C, which acts as a tool for tuning the shape fixity of the specimens (Kolesov et al. 2015; Argun et al. 2019; Zeng et al. 2021).

The soft domain  $T_g$  transition of each specimen is also shown in Fig. 3c. A significant difference in this figure is the sharp increase in PCL segments'  $T_g$  value for the PCL-tPU compared to PCL-TPPU, which confirms the fact that chemical confinement of polyol between CNW reduces their mobility. Another interesting phenomenon that has occurred is that the  $T_g$  values of the thermoset PU specimens composed of both PCL and PTMG segments are lower than the  $T_g$  values of the soft segments composed of only PCL<sub>2000</sub> or PTMG<sub>2000</sub>. They have also shown higher  $\tan\delta$  peak height. Neat PCL's  $T_g$  is around  $-61 \pm 1$  °C, while for PTMG the  $T_g$  value is  $-65$  °C (Bershtein et al. 2005; Zhuravlev et al. 2011). Compared to PCL<sub>2000</sub> and PTMG<sub>2000</sub> segments, both polymers have experienced an increase of about  $+14$  °C in their  $T_g$ s once they are used in the thermoset PU/CNW structure. Chemical confinement of the polyols restricts the soft segments' motion and reducing the ease of soft segment rotation. The declined segmental motion of the PCL<sub>2000</sub> and PTMG<sub>2000</sub> segments in the PCL-tPU and PTMG-tPU specimens is responsible for the  $+14$  °C increase in their  $T_g$ . The interesting fact is that both the PCL<sub>2000</sub> and PTMG<sub>2000</sub> soft segments have experienced almost the same extent of increase. The negligible variation can be due to the small difference in their chain flexibility as indicated by the 4 degrees difference in their  $T_g$ . The reason behind the lower values of  $T_g$ s for soft domain chains with different combinations of PCL and PTMG segments can be explained by their increased chain dynamics (Jafari et al. 2020). The lower  $T_g$  values indicate higher segmental mobility as it manifests itself in the slight increase in  $\tan\delta$  peak heights related to the specimens. For the thermoset PUs, the lowest  $T_g$  value corresponds to the Blend-tPU specimen, with

soft domains composed of PCL<sub>2000</sub> and PTMG<sub>2000</sub>, and the highest  $\tan\delta$  peak height is also corresponds to this specimen. The soft domain of the Blend-tPU specimen is composed of incompatible segments and the single  $\tan\delta$  peak behavior of the soft domain indicates their increased miscibility. The increase in phase miscibility of two semi-crystalline polymers results in a decrease in order and consequently a decline in their crystallization ability. The same concept is applicable for Block 1:1-tPU and mixture-tPU specimens. The impact of morphological and compositional complexity on crystallization potential of the soft domain chains will be discussed later in the DSC and XRD results.

## Soft domain crystallization

### DSC analysis

For a system of two incompatible semi-crystalline segments, the characteristic crystallization parameters provide insights into the phase organization of the segments. The results of crystallization analysis for the used polyols are shown in Fig. 4a, b, and the characteristic parameters are summarized in Table 2. Based on the results, PCL<sub>2000</sub> has the highest crystallization ( $T_c$ ) and melting ( $T_m$ ) temperatures of  $26.6$  and  $51.7$  °C, respectively. PTMG<sub>2000</sub> has a  $T_c$  and  $T_m$  of  $12.8$  and  $25.7$  °C, respectively. Block copolymerization of these two polymers with PCL<sub>1000</sub>-PTMG<sub>2000</sub>-PCL<sub>1000</sub> architecture has led to two distinct crystallization peaks at  $18.5$ ,  $8.3$  °C and three melting peaks at  $39.3$ ,  $33.7$ , and  $22.8$  °C. Besides the depression of crystallization and melting peak points for both polymer segments, the crystallization enthalpies has also experienced a decline compared to PCL<sub>2000</sub> and PTMG<sub>2000</sub> homopolymers. Regarding the  $T_c$ s, the peak points of  $+18.5$  and  $+8.3$  °C correspond to PCL<sub>1000</sub> and PTMG<sub>2000</sub> blocks, respectively. As a general fact, block copolymerization of two semi-crystalline polymers reduces their thermal stability through changing their crystallites' morphology, which is dependent on their block lengths (Nojima et al. 1995; Müller et al. 2002). The melting temperatures of  $39.3$  and  $33.7$  °C correspond to PCL segments and the peak at  $22.8$  °C is related to the PTMG<sub>2000</sub> block. The higher  $T_c$  value of the PCL indicate that its crystallites have a higher

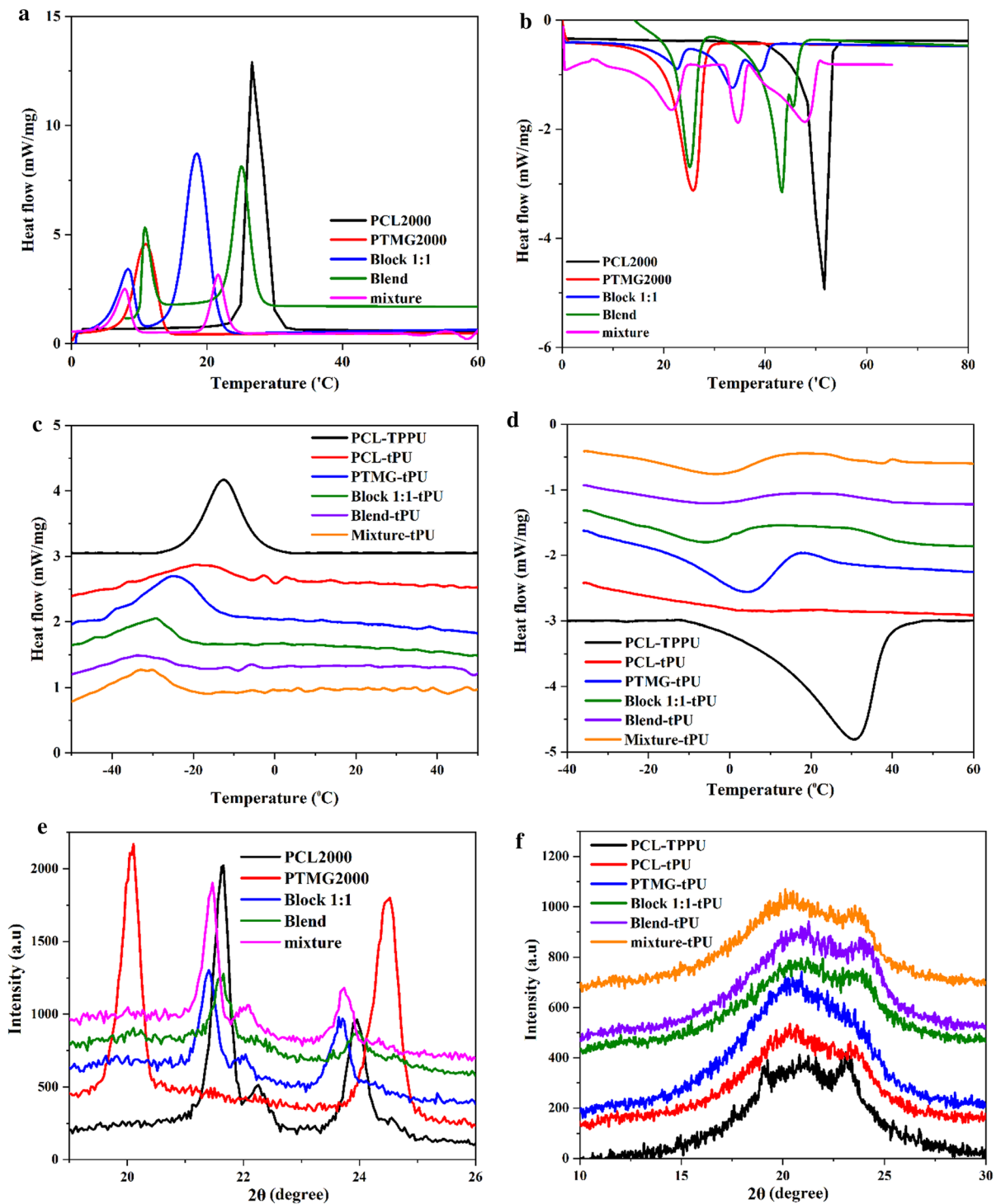


**Fig. 4** The DSC thermograms of the polyols and the thermoset PUs: **a** second heating and **b** cooling regime of the polyols; **c** second heating and **d** cooling regime of the tPUs. The X-ray

diffraction spectrum of **e** the polyols and **f** the thermoset PU/CNW nanocomposites

**Table 2** The crystallization and melting temperatures of the polyols and the soft segments in the thermoplastic PCL-based PU and the thermoset PU structure

Sample	T <sub>c</sub> (°C)	T <sub>m</sub> (°C)	Sample	T <sub>c</sub> (°C)	T <sub>m</sub> (°C)
PCL <sub>2000</sub>	26.6	51.7	PCL-TPPU	− 14.2	31.0
–	–	–	PCL-tPU	− 18.0	3.1
PTMG <sub>2000</sub>	12.8	25.7	PTMG-tPU	− 25.0	4.1
Block 1:1	18.5, 8.3	39.3, 33.7, 22.8	Block 1:1-tPU	− 29.5	− 5.9
Blend	25.0, 10.8	45.7, 43.3, 25.0	Blend-tPU	− 33.0	− 4.4
Mixture	21.6, 7.9	47.4, 34.5, 22.0	mixture-tPU	− 32.0	− 2.4

thermal stability compared to the PTMG crystallites, which leads to its higher crystallization kinetics. Therefore, due to its higher T<sub>c</sub> value, the PCL segments would first undergo crystallization, as their crystallites nucleation starts at higher temperatures, leading to increased phase segregation. Early crystallization of PCL segments would affect the PTMG crystallization and increase the imperfectness of its crystallites. The covalent bonding of the PCL<sub>1000</sub> and PTMG<sub>2000</sub> blocks in an ABA architecture limits their phase separation and increases disorder in the block copolymer chain. These structural features affect the crystallites' morphology and thermal stability of both crystallizable blocks. The limited phase separation of the PCL-PTMG blocks alongside with early crystallization of PCL segments reduces the conformational entropy of PTMG segments and their ability to fold and form stable crystallites.

The depression in the characteristic temperatures are lesser in the Blend sample, which comprises of 1:1 w:w PCL<sub>2000</sub>:PTMG<sub>2000</sub> homopolymers. The PCL<sub>2000</sub> and PTMG<sub>2000</sub> chains are not covalently connected to each other and upon cooling they can easily separate and form relatively stable crystallites and the characteristic crystallization would not be impacted greatly. The reason for the decline in the characteristic temperatures is a combination of kinetics and thermodynamics effects (Zakizadeh et al. 2021). The kinetics works in the course of crystallization and impacts the lamella thickness (L), which is related to T<sub>m</sub> through Eq. 5. This equation indicates that the lower L results in lower T<sub>m</sub> (Castillo and Müller 2009; He and Xu 2012).

$$T_m = T_m^0 \cdot \left( 1 - \frac{2v_e}{\Delta H_f L} \right), \quad (5)$$

Here,  $v_e$  is the free energy of chain folding at the lamella's surface and  $\Delta H_f$  is the lamella heat fusion.

As mentioned earlier, covalent bonding of the two incompatible polymers limits their phase separation and this structural feature affects the crystallites' morphology and predominantly reduces L and a reduction in T<sub>m</sub> of each block would be a direct result of this change (Chen et al. 2001). From thermodynamic point of view, the controlling parameter of the changes in thermal stability of the crystallites is the product of the interaction parameter ( $\chi_{AB}$ ) and the block lengths (N), i.e.  $\chi_{AB} \cdot N$ . For higher block lengths the impact of covalent bonding on the characteristic temperatures would be lower (Vilgis and Halperin 1991).

For the mixture specimen, the depression in T<sub>c</sub> and T<sub>m</sub> of PCL segments are not very large compared to the Block 1:1 specimen. The reason for the relatively higher T<sub>c</sub> and T<sub>m</sub> of PCL segments can be defined as follows: higher crystallization temperature of PCL segments compared to PTMG segments results in their early crystallization, which results in crystallization-assisted phase separation of PCL segments. Presence of the block copolymer reduces the interfacial tension between the incompatible PCL and PTMG domains, hence, reducing the extent of phase separation and resulting in smaller domains of PCL and PTMG (Müller et al. 2002; He and Xu 2012).

Regarding the PCL-TPPU and the thermoset PU-CNW specimens, as their crystallization and melting spectrum are represented in Fig. 4c, d, the polyols as soft segments have experienced an enormous decline in their crystallization potential. As a general fact, incorporation of semi-crystalline polyols into polyurethane structure leads to a decline in their crystallization ability, however, as reported in our previous paper (Jafari et al. 2020), thermoset PUs of PEG-PCL polyols with CNWs had a larger impact compared to their thermoplastic counterparts. Based on Fig. 4c, d, the PCL-TPPU had a higher T<sub>c</sub> and T<sub>m</sub> values

compared to its thermoset PU counterpart, which is in agreement with our previous results. The reasons behind the sharp declines are: (1) chemical attachment of the polyol chains to CNWs, which highly limits their mobility and kinetics of crystallization, and (2) the repulsive interaction between the polyols and the urethane functionalities (Saralegi et al. 2013; Shirole et al. 2018; Khadivi et al. 2019).

According to the summarized data in Table 2, the Blend-tPU, Block 1:1-tPU and mixture-tPU specimens have negative  $T_m$  values and their  $T_c$  values are the lowest compared to tPUs of PCL<sub>2000</sub> and PTMG<sub>2000</sub>. This result is in accordance with the results shown for the polyols as block copolymerization and blending reduces the thermal stability of the crystallites. Therefore, the adverse impact of thermosetting on these soft segments would be higher.

### X-Ray diffraction analysis

The XRD analysis provides information on the structure of the crystallites' unit cells and the impact of crystallites' perfection or defects can be seen as the changes in their  $2\theta$  positions, the width and the intensity of the peaks. Based on Bragg's law, Eq. 6, the change in  $2\theta$  positions directly changes the d-spacing (Nourany et al. 2021; Noormohammadi et al. 2021).

$$n\lambda = 2d\sin(\theta), \quad (6)$$

According to Fig. 4e, the PCL<sub>2000</sub> polyol showed diffraction peaks at  $2\theta = 21.65^\circ$ ,  $22.22^\circ$ , and  $23.95^\circ$ , which are attributed to the 110, 111 and 200 planes (Hoidy et al. 2010). PTMG<sub>2000</sub> showed two diffraction peaks at  $2\theta = 20.10^\circ$  and  $24.52^\circ$  corresponding to d-spacing of 0.42 and 0.38 nm. According to the literature, block copolymerization of semi-crystalline polymers reduces their crystallization extent and as a direct result  $T_c$  and  $T_m$  decreases, which is an indication of lowered thermal stability of the crystallites. For the PCL<sub>1000</sub>-PTMG<sub>2000</sub>-PCL<sub>1000</sub> block copolymer with hydroxyl end-groups (Block 1:1), the intensity of the diffraction peaks related to the PCL<sub>1000</sub> blocks ( $2\theta = 21.40^\circ$ ,  $22.03^\circ$  and  $23.73^\circ$ ) have declined by about half compared to PCL<sub>2000</sub> homopolymer and the peaks related to PTMG<sub>2000</sub> have almost disappeared except for the peak available at  $2\theta = 20.18^\circ$ , with extremely low intensity. The results indicate that the block copolymerization had

a higher impact on the middle block (PTMG<sub>2000</sub>). The reason behind this result can be the higher  $T_g$  of PTMG compared to PCL and consequently lower chain dynamics, which affects its crystallization kinetics. The changes in  $2\theta$  degrees show the structural changes of crystallites' unit cells as the blocks are covalently attached and affect the nature of the crystallites' morphology and their development (Jiang et al. 2001; Luyt and Gasmi 2016).

For the Blend polyol (1:1 w:w PCL<sub>2000</sub>/PTMG<sub>2000</sub> blend), the peak positions have not experienced any significant change and only the diffraction peaks' intensities have declined. This is due to the fact that the two incompatible semi-crystalline polymers have not affected the crystallization thermodynamics and only crystallization kinetics has been impacted (Luyt and Gasmi 2016). Compared to the homopolymers, for the mixture (the relative 1:1:1 weight ratios of PTMG<sub>2000</sub>, PCL<sub>2000</sub> and the block copolymer), the diffraction peak positions have shifted towards lower diffraction peaks ( $2\theta = 21.46$ ,  $22.10$ , and  $23.73$  with a broad peaks at  $20.18^\circ$ ). Addition of the block copolymer into the blend reduces the interfacial tension between the two phases. This change improves the phase miscibility of the PCL and PTMG segments at the interface and limiting the extent of phase separation.

As seen in Fig. 4c, d, the PCL-TPPU specimen showed higher  $T_c$  and  $T_m$  values compared to the thermoset PU/CNW nanocomposites, which is attribute to higher mobility restriction imposed on soft segments through chemical cross-linking by CNWs with numerous active structural -OH groups. The thermoplastic PU showed  $2\theta$  peaks at  $19.09$ ,  $19.96$ ,  $21.66$  and  $23.07$ , which shows the availability of the PCL crystallites at room temperature. The first two peaks are related to formation of hard segment crystallite and the latter two peaks corresponds to PCL crystallites. Regarding the PU/CNW thermosets, the crystallization ability and the thermal stability of the crystallites has reduced to a large degree. Based on Fig. 4f, the overall shape of the spectrums are broad indicating the amorphous nature of the soft segments at room temperature. Presence of a distinguishable peak at  $2\theta$  of  $23.4^\circ$  is related to the characteristic diffraction peak of CNW (Noormohammadi et al. 2021). The 1.0 wt% content of the CNW allows for detection of their crystallites' structure.

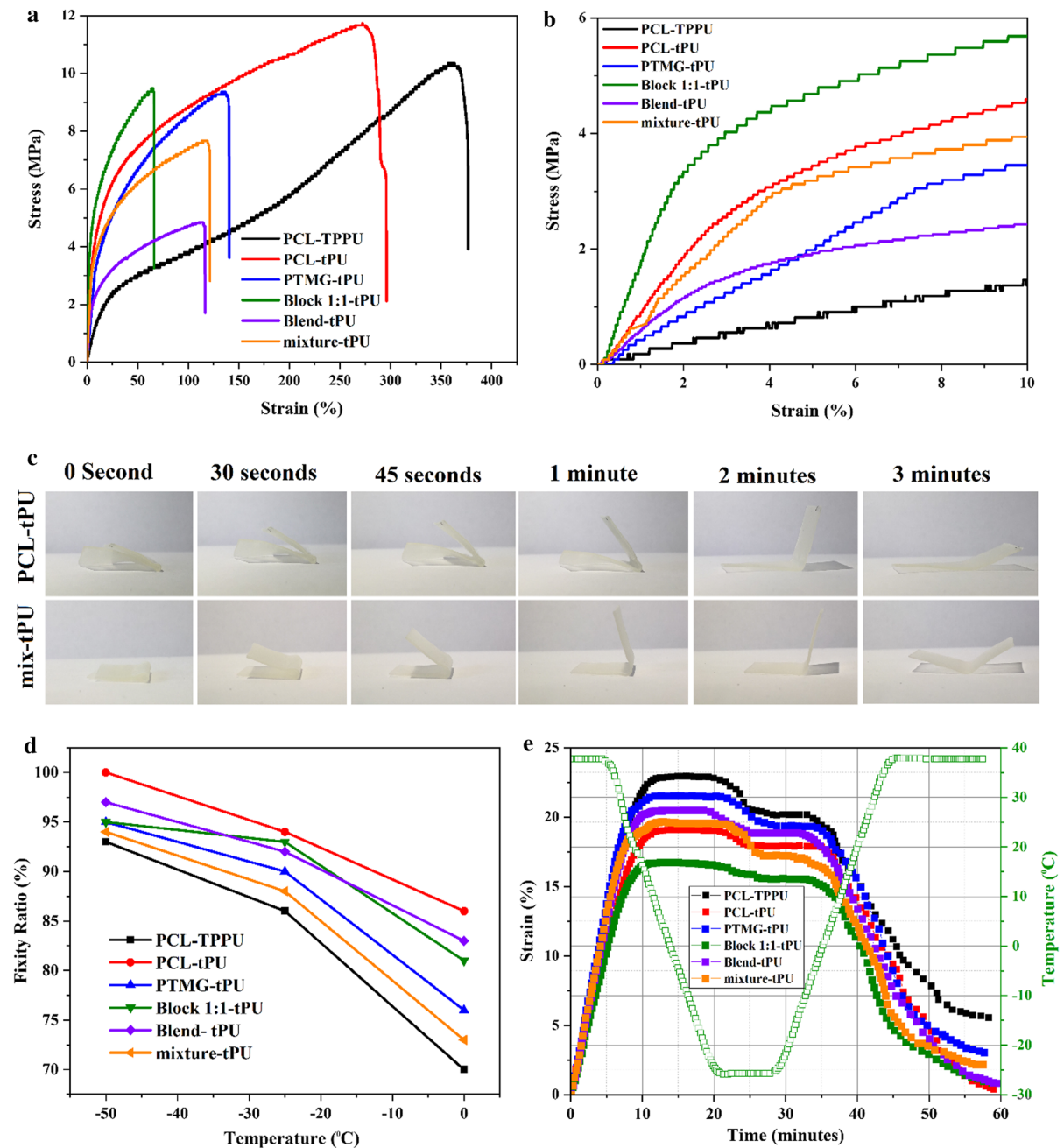


**Fig. 5** The stress–strain behavior of the thermoplastic PCL-based PU and the thermoset PU/CNW nanocomposites **a** in full-scale and **b** low-strain scale. **c** Digital photographs of the PCL- and mixture-tPUs recovering at room temperature, **d**

shape fixity ratio as a function of temperature, and **e** the shape memory process of the thermoset PU nanocomposites fixed at  $-25\text{ }^{\circ}\text{C}$  with the recovery temperature of  $+37.5\text{ }^{\circ}\text{C}$

### Mechanical properties

Since the thermoset PU/CNW nanocomposites do not contain any stable soft segment crystallites at room

temperature, they can be considered as rubbers and their deformation under a uniaxial stretching should follow the thermodynamics of rubbers (Vorov et al. 2008).

**Table 3** The characteristic mechanical properties of the thermoplastic PCL-based PU and the thermoset PU/CNW nanocomposites

Specimen	$\varepsilon_u(\%)$	$\sigma_u(\text{MPa})$	E (MPa)	$\nu \times 10^7(\text{mol}/\text{cm}^3)$
PCL-TPPU	$367.2 \pm 11.4$	$10.35 \pm 0.42$	$16.5 \pm 2.8$	–
PCL-tPU	$289.0 \pm 7.1$	$11.67 \pm 0.39$	$100.1 \pm 3.6$	$23.9 \pm 1.3$
PTMG-tPU	$140.4 \pm 5.6$	$9.27 \pm 0.17$	$40.7 \pm 2.1$	$24.2 \pm 0.5$
Block 1:1-tPU	$66.2 \pm 3.9$	$9.48 \pm 0.13$	$166.9 \pm 5.8$	$13.7 \pm 0.8$
Blend-tPU	$116.5 \pm 4.2$	$4.85 \pm 0.15$	$56.4 \pm 3.7$	$22.8 \pm 1.1$
Mixture-tPU	$121.4 \pm 5.0$	$7.66 \pm 0.21$	$73.9 \pm 2.9$	$19.4 \pm 0.9$

$$f = \left(\frac{\partial U}{\partial L}\right)_{T,V} + T \left(\frac{\partial f}{\partial T}\right)_{V,L} = f_E + f_S, \quad (7)$$

Based on Eq. 7, the force  $f$  applied to the PUs comprises of two factors, energetic and entropic contributions. Since the nanocomposites have amorphous state at room temperature,  $f_E \cong 0$  and the entropic contribution is more dominant. The energetic contribution is more dominant in highly crystalline specimens in which stretching distorts the lattice spacing. At constant temperature, upon stretching the specimens, the soft segments face a decline in their conformational entropy and according to Eq. 8, the required force for further stretching increases (Stribeck et al. 2015). According to Fig. 5a, this behavior is seen for the majority of the specimens, especially for the PCL-TPPU which shows strain-hardening behavior at higher extensions.

$$f_S = T \left(\frac{\partial f}{\partial T}\right)_{V,L} = -T \left(\frac{\partial S}{\partial L}\right)_{T,V}, \quad (8)$$

Overall, at low strains,  $\lambda < 1$ , the energetic contribution is negligible and the entropic contribution dominates. Based on Fig. 5a and Table 3, among the thermoset PU nanocomposites, PCL-tPU had the highest elongation at break ( $\varepsilon_u$ , ultimate strain) of 289.0% and ultimate stress ( $\sigma_u$ ) of 11.67 MPa, while PTMG-tPU had an  $\varepsilon_u$  and  $\sigma_u$  of 140.4% and 9.27 MPa, respectively. The  $\varepsilon_u$  of the block 1:1-tPU declines sharply with a value of 66.2% despite of having a higher soft segment length or higher molecular length between cross-link points (Mc). The Blend-tPU and mixture-tPU specimens have also experienced an intense decline in their  $\varepsilon_u$  and besides this change, their  $\sigma_u$  have also declined with a  $\sigma_u$  of 4.85 MPa for the Blend-tPU. Regarding the Young's modulus (E), as summarized in Table 3, Block 1:1-tPU specimen

has the highest E value of 166.9 MPa. The E values are measured from the low-strain linear elastic regions of the stress–strain curves (Fig. 5b, below 2% strain). For a uniaxial deformation of a cross-linked system with the assumption of  $\Delta V \cong 0$ , no change in volume upon stretching, we have Eq. 9:

$$G = \frac{nkT}{V} = \nu kT = \frac{\rho RT}{M_s}, \quad (9)$$

Based on this general equation for a network of a homopolymer, the modulus of the specimen increases as a linear function of number density of the strands (an increase in strand length decreases the number of strands per unit volume) (Vorov et al. 2008; Scetta et al. 2021). However, by looking at cross-link density (CLD,  $\nu$ ) of the specimens summarized in Table 3, it can be seen that the Block 1:1-tPU has the lowest CLD value but showed the highest modulus of 166.9 MPa. As the chemistry and configuration of soft domain chains differ, the Eq. 8 that has been developed for simple networks in uniaxial deformations fails to predict the overall trend of the mechanical behavior.

One possible explanation for the peculiar behavior can be found in the elastic modulus of the specimens at room temperature. According to Fig. 4a, the E' of PTMG-tPU and mixture-tPU are around 30 and 60 MPa, respectively. However, the E' values of the remaining specimens are in the range of 100–200 MPa, which are roughly in correlation with the Young's modulus of the specimens. The rod-like morphology of the highly crystalline CNW, which creates an asymmetry in the system, and its chemical bonding to the prepolymer chains would have also played a key role in controlling the mechanical properties of the thermoset PU/CNW nanocomposites.

The Young's modulus of the thermoplastic PUs, depending on the curing process and the nature of

the Diisocyanate, is usually below 10 MPa (Tito et al. 2019; Xiang et al. 2021). The high  $E$  values of the thermoset PU/CNW nanocomposites compared to PCL-TPPU and other thermoplastic PUs reported in the literature suggests that the CNWs, as high-modulus rod-like nanoparticles, have played a key role in increasing the strength and elasticity of the thermoset PUs. As shown in SEM images, the CNWs are dispersed in the matrix in a relatively uniform way, which is due to the fact that the chemical bonding of the nanoparticles to the prepolymer prohibits their self-assembly and further clustering.

### Shape memory performance

According to Fig. 5c, the digital photographs of the PCL-tPU and mixture-tPU specimens that are fixed in liquid  $N_2$  and their recovery process was performed at room temperature. The images show that the folded specimens have unfolded to a large degree. In a more systematic study, the glass transition phenomena is usually considered as the base for selection of the fixity temperature (Garle et al. 2012; Zeng et al. 2021). In this research, the three different temperatures of  $-50$ ,  $-25$  and  $0$  °C were selected for evaluation of the fixity ratio ( $R_f$ ). Figure 5d shows the change in  $R_f$  as a function of temperature for each specimen. The results indicate that as the temperature increases, the ability of the specimens to fix their temporary shape declines. The reason for this change is the gradual decline of elastic modulus after the  $T_g$  transition and an increase in soft segment entropy, which tends to regain the relaxed state (Gao et al. 2018; Nessi et al. 2019; Zare et al. 2019; Du et al. 2021). For amorphous polymers, the decline in elastic modulus after  $T_g$  is sharp and the temperature dependency of  $R_f$  is

not very strong. However, for the tPUs with semi-crystalline nature, the temperature dependency of  $R_f$  is strong due to the broad  $T_g$  transition and the specimens are considered to consist of an infinite number of nano-domains with corresponding  $T_g$ s (Zhang et al. 2019a; Gupta and Mekonnen 2022). The broad  $T_g$  transition allows for tuning the fixity ratio as the nano-domains with higher  $T_g$  values are able to freeze the stored entropic energy (Liu et al. 2015; Mi et al. 2018; Khadivi et al. 2019; Nourany et al. 2021; Ranjbar et al. 2021). Based on the results, the highest shape fixity of 100% corresponds to PCL-tPU at  $-50$  °C, which is due to the fact that this temperature is below its  $T_g$  peak value and the soft segments lack any elastic recovery (Chen et al. 2010; Yu et al. 2014; Wu et al. 2014). According to the literature, elastic modulus is responsible for controlling shape fixity and crystallization of the soft segments, as a key factor, also increase the elasticity of the specimens in the plateau region (Kumar Patel and Purohit 2018; Argun et al. 2019). At the temperature of  $-25$  °C, the  $R_f$  is still high for all the specimens, which is due to the fact that melting temperatures of the existing crystallites are well above this temperature. The temperature of  $0$  °C is very close to  $T_m$  of the crystallites, slightly below or above  $T_m$  for each specimen, which in turn cause a sharp decline in  $R_f$ , as shown in Fig. 5d. Figure 5e shows the DMA results of the shape memory performance analysis for the shape fixity temperature of  $-25$  °C and the recovery temperature of  $+37.5$  °C. According to the DMTA results, the thermoset specimens possessed a high elastic modulus (above 30 MPa) even at higher temperatures, which is due to the thermoset nature of the specimens and the presence of the high modulus CNW nanoparticles. However, the PCL-TPPU specimen with thermoplastic nature showed an intense decline in its elastic modulus, which leads to an increased potential of the specimen to dissipate the stored elastic energy. According to Table 4, the PCL-TPPU showed a low recovery ratio of 75%, which is due to the high entropic energy dissipation caused by higher mobility of the chains. Based on Table 4 and Fig. 5e, regarding to the thermoset PUs, the PTMG-tPU and mixture-tPU specimens showed relatively low recovery ratios. The remaining three thermoset specimens showed very high recovery ratios falling in the range of 95–98%. The reason for the high  $R_f$  of the three specimens can be their high and stable elastic modulus compared

**Table 4** The shape memory parameters of the synthesized thermoset PU nanocomposites fixed at  $-25$  °C with recovery temperature of  $+37.5$  °C

Specimen	Fixity ratio (%)	Recovery ratio (%)	X-link degree (%)
PCL-TPPU	87	75	–
PCL-tPU	94	98	$97 \pm 1$
PTMG-tPU	90	86	$98 \pm 1$
Block 1:1-tPU	93	95	$96 \pm 2$
Blend-tPU	92	96	$97 \pm 1$
Mixture-tPU	88	89	$98 \pm 2$



to the other two specimens. The advantage of thermoset PUs over thermoplastic PUs is their constant elastic modulus at elevated temperatures and over a wide temperature range, which is a sign of a constant entropic driving force for recovering the original shape (Sarkhosh et al. 2021).

In a PU structure, the soft domain is the active phase for recovering the original shape and upon stretching the specimens at elevated temperatures, the chains in the active phase experience a decline in their conformational entropy (Jiu et al. 2016; Zhang et al. 2019b). By keeping the applied force and decreasing temperature, parts of the stretched chain segments are aligned in the crystalline structures (Barot et al. 2008; Bouaziz et al. 2017). Upon removing the force at  $-25\text{ }^{\circ}\text{C}$ , since the temperature is well above the  $T_g$  transition peak, the specimens experience a partial spontaneous shape recovery. However, as the temperature increases, the segments tend to increase their conformational entropy and shrink in size (Zhou et al. 2014; Zhang et al. 2019a), which in our case it is expressed as a decrease in longitudinal length. For a thermoset system, the most important parameter in determining the shape recovery ratio is the cross-link degree and density, which provides a network point for reducing the chain slippage and energy dissipation ability of the soft segments (Li et al. 2018; Gao et al. 2018). In reality, achieving an ideal chemical network is practically impossible. However, the CNWs with abundant hydroxyl groups were able to create a high cross-linking degree being in the range of 96–98%. The reason for the high and close to each other can be the abundance of hydroxyl groups, which serve as the cross-linking point for the prepolymers (Nourany et al. 2021; Ranjbar et al. 2021). Since the cross-linking degrees of the thermoset PUs were high and close to each other, the elastic modulus was considered to be the main parameter in determining the final shape recovery at the experimental time period.

### Surface topography analysis

The surface physics of biomaterials, including surface roughness and uniformity, is a key feature that affects adhesion of seeded cells. For the thermoset PU/CNW nanocomposites, the physical features of the surface can also provide information on the possible clustering of the CNWs. Since CNWs are highly hydrophilic and due to the hydrogen bonding between

the nanorods, formation of CNW clusters is a common phenomenon in hydrophobic matrixes. Prohibiting clustering of nanorods can highly increase their reinforcement effect (Noormohammadi et al. 2021). Regarding the surface features, Average roughness,  $R_a$  (Eq. 10), and Root Mean Square (RMS) roughness, ( $R_q$  Eq. 11), are the statistical representations of deviation and standard deviation in the surface height of each substrate. Skewness,  $R_{Sk}$  (Eq. 12), which is statistically expressed as the third moment of profile amplitude probability density function ( $z_i - \bar{z}$ ), is an indication of the deviation in the surface height symmetry from normal distribution. The normal distribution is mathematically defined as  $R_{Sk} = 0$ , and a positive Skewness physically indicates presence of more peaks than valleys and planar structures. The surface sharpness, expressed by Kurtosis ( $R_{Ku}$ , Eq. 13), is obtained by taking the fourth moment of ( $z_i - \bar{z}$ ) and the value of 3 represents a surface with Gaussian amplitude distribution. The higher values represent the predominant peaks and as the value increases the sharpness of the peaks also increases (Kumar et al. 2011; Landa et al. 2014).

$$R_a(N, M) = \frac{1}{NM} \sum_{x=1}^N \sum_{y=1}^M (z(x, y) - \bar{z}(N, M)) \quad 3D, \quad (10)$$

$$R_q(N, M) = \sqrt{\frac{1}{NM} \sum_{x=1}^N \sum_{y=1}^M (z(x, y) - \bar{z}(N, M))^2} \quad 3D, \quad (11)$$

$$R_{Sk} = \frac{1}{NR_q^3} \sum_{i=1}^N [z_i - \bar{z}]^3, \quad (12)$$

$$R_{Ku} = \frac{1}{NR_q^4} \sum_{i=1}^N [z_i - \bar{z}]^4; \quad (13)$$

Figure 6 shows the topographical 3D images of the substrates' surface in two different scales of 10 and 2  $\mu\text{m}$ . The statistical information of the surface topography is summarized in Table 5. The results indicate that all the PU specimens show a positive skewness, which is an indication of a surface with predominant peaks. The average roughness ( $R_a$ ) falls in the range of 16.21–26.0 nm, which is a relatively narrow range. The AFM topographical 3D images with the scale of 2  $\mu\text{m}$  (right column) provide a better

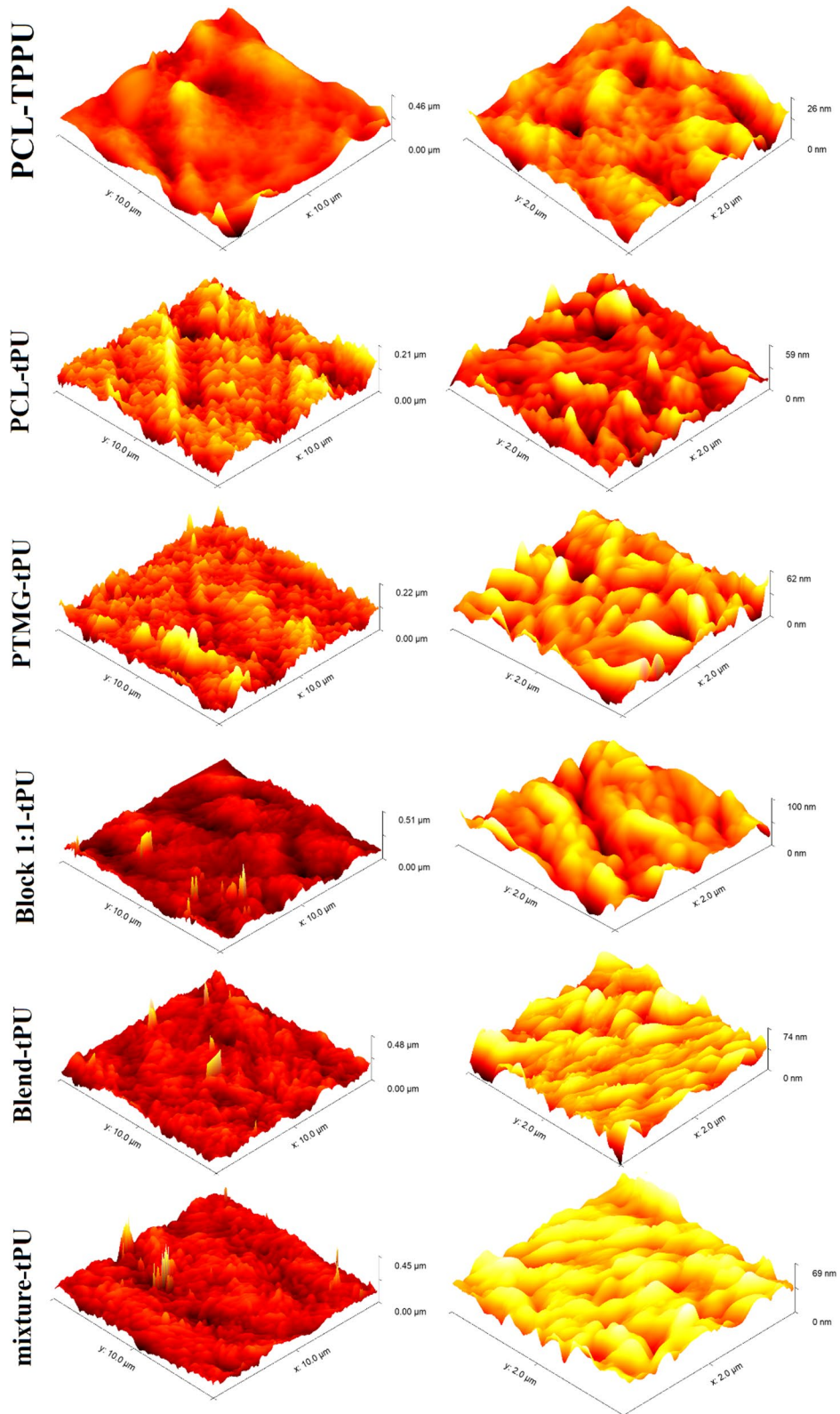


**Fig. 6** The 3D topographical surface images of the thermoset PUs at room temperature

visual perspective into the morphology of the peaks. As it can be seen, for the PU/CNW thermosets, the morphology of the peaks have changed compared to PCL-TPPU. The peaks have an elongated morphology, which might be due to the existence of CNWs close to the surface, as seen in the SEM surface images (third row).

**Table 5** The characteristic statistical parameters of the topological AFM images

Sample	$R_a$ (nm)	$R_q$ (nm)	$R_{Sk}$	$R_{Ku}$
PCL-TPPU	16.21	19.35	0.121	0.302
PCL-tPU	20.10	25.68	0.158	0.586
PTMG-tPU	17.69	23.26	0.742	1.954
Block 1:1-tPU	26.00	33.45	0.419	1.014
Blend-tPU	22.92	29.57	0.554	1.609
mixture-tPU	22.91	29.71	0.218	0.701

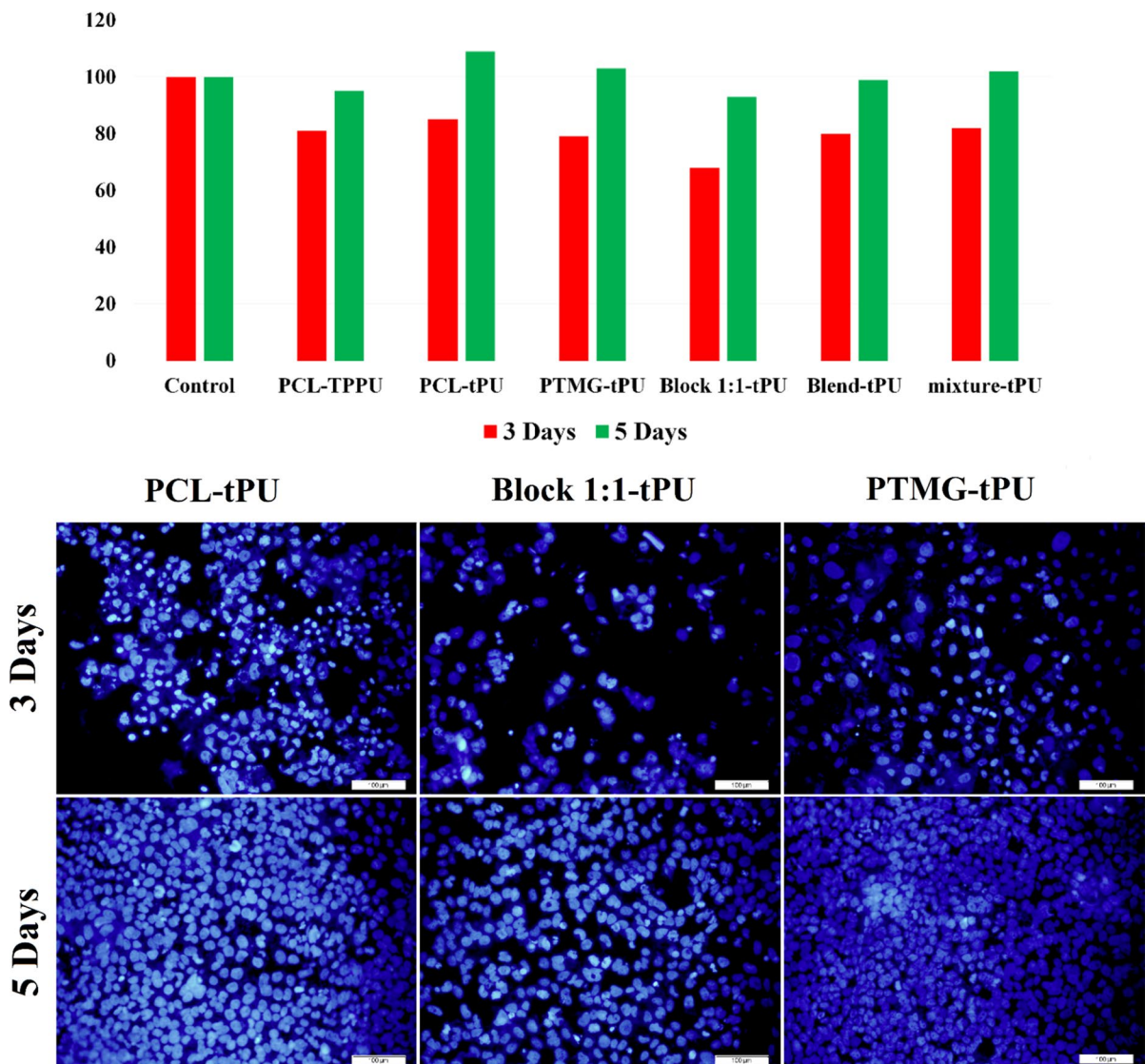


**Fig. 7** (Top) MTT assay using HFF cells cultured on the thermoplastic PCL-based PU and the thermoset PU/CNW nanocomposites for 3 and 5 days. (Bottom) Fluorescent images of the cell-seeded films after 3 and 5 days of culturing HFF cells

According to Table 5, the Block 1:1-tPU had the highest RMS roughness of 33.45 nm and the PCL-TPPU had the lowest RMS roughness being equal to 19.35 nm. The  $R_{sk}$  values are not very high and are close to the normal surface height distribution. The low  $R_{ku}$  values of the thermoset PU/CNW nanocomposites indicate that the surface is inclined towards flatness and the surface peaks are not very sharp (Behrouz et al. 2022).

The reason for the relatively higher roughness and predominant peaks in the thermoset PU/CNWs is related to the presence of CNWs on the surface, which are seen in the topographical images presented in Fig. 6.

### Cell culture analysis

MTT assay is performed on the specimens using HFF cells to evaluate their cytotoxicity. The viability of the cells on the specimens relative to the control TCPS culture plate is considered as a basis for evaluating the cytotoxicity of the specimens (Nourany et al. 2021). Based on the statistical results of the MTT assay presented in Fig. 7 (top image), in the first three days of the culturing, the cell growth on the specimens, being around 76%, compared to the control is low. The lowest cell growth is for Block 1:1-tPU with a relative cell growth of 68%. The reason for the lower relative cell growth can be the induction time for cell attachment (Ranjbar et al. 2021). After 5 days of cell culture, the seeded HFF cells tend to grow with an average relative cell growth of 102%. The lowest cell growth was again corresponded to the Block 1:1-tPU specimen with a relative cell growth of 93%. The low cell viability of the Block 1:1-tPU can be related to the presence of free CNWs as this specimen has the lowest cross-link density.

Overall, the cell viability of 90% or higher for the materials is considered non-toxic and based on the results of 5 days of culture, the specimens are considered to be highly biocompatible (Nourany et al. 2021). The fluorescent images of PCL-tPU, Block 1:1-tPU and PTMG-tPU are shown in Fig. 7, which indicate that the cell density and growth is higher for PCL-tPU and PTMG-tPU. Based on the images, the cell density of the Block 1:1-tPU is lower compared to other specimens.

### Conclusion

The results of shape memory analysis indicated that the thermoset PUs possessed high  $R_f$  values falling in the range of 86–98%, while the PCL-based thermoplastic PU showed a low  $R_f$  value. The higher  $R_f$  values of the thermoset PUs is related to their thermoset nature and lack of chain slippage. There was a direct correlation between the storage modulus ( $E'$ ) and  $R_f$  values as the thermoset PU/CNW nanocomposites showed stable and high  $E'$  values at temperatures above 20 °C. The  $\tan\delta$  peak height of the thermoset specimens was below 0.14, while the high  $\tan\delta$  value of 0.35 for the TPPU is an indication of high chain mobility, which favors loss of stored elastic energy. The results of shape fixity ( $R_f$ ) analysis indicated the temperature-dependency of this parameter, which was due to the broad  $T_g$  transition caused by chemical cross-linking and crystallinity of the soft segments. The higher  $E'$  values of tPUs compared to PCL-TPPU at low temperatures showed their improved ability in freezing the stored elastic energy. The high biocompatibility and HFF cell growth proved the successful development of new biomaterials with multi-functional role.

**Acknowledgments** We would like to thank Seyed Sadi Hosseini for his insightful comments on the cytotoxicity analysis.

**Author contribution** EA: Data acquisition, data validation, formal analysis, writing the original draft; MAM, SB, FN: Data validation, formal analysis, editing the original draft; YRD: Data acquisition, formal analysis; MN: Conceptualization, data validation, writing the original draft, funding and grant acquisition.

**Funding** This work was partially funded by Amirkabir University of Technology and the grant number is not applicable.

**Data availability** The experimental data will be provided by the corresponding author upon reasonable request.

### Declarations

**Conflict of interest** The authors have no conflict of interest.

### References

Argun A, Gulyuz U, Okay O (2019) Semi-crystalline, three-segmented hybrid gels with multiple shape-memory

- effect. *Macromol Symp* 385:1800164. <https://doi.org/10.1002/masy.201800164>
- Barot G, Rao IJ, Rajagopal KR (2008) A thermodynamic framework for the modeling of crystallizable shape memory polymers. *Int J Eng Sci* 46:325–351. <https://doi.org/10.1016/j.ijengsci.2007.11.008>
- Behrouz T, Behrooz S, Sarkhosh H, Nourany M (2022) A novel multi-functional model thermoset and PDA-coated PU nanocomposite based on graphene and an amphiphilic block copolymer. *Polym Adv Technol*. <https://doi.org/10.1002/pat.5703>
- Bershtein VA, David L, Egorov VM et al (2005) Structural/compositional nanoheterogeneity and glass-transition plurality in amorphous polycyanurate–poly(tetramethylene glycol) hybrid networks. *J Polym Sci Part B Polym Phys* 43:3261–3272. <https://doi.org/10.1002/polb.20614>
- Bouaziz R, Roger F, Prashantha K (2017) Thermo-mechanical modeling of semi-crystalline thermoplastic shape memory polymer under large strain. *Smart Mater Struct* 26:55009. <https://doi.org/10.1088/1361-665x/aa6690>
- Cao F, Jana SC (2007) Nanoclay-tethered shape memory polyurethane nanocomposites. *Polymer (Guildf)* 48:3790–3800. <https://doi.org/10.1016/j.polymer.2007.04.027>
- Castillo RV, Müller AJ (2009) Crystallization and morphology of biodegradable or biostable single and double crystalline block copolymers. *Prog Polym Sci* 34:516–560. <https://doi.org/10.1016/j.progpolymsci.2009.03.002>
- Chen H-L, Hsiao S-C, Lin T-L et al (2001) Microdomain-tailored crystallization kinetics of block copolymers. *Macromolecules* 34:671–674. <https://doi.org/10.1021/ma001485e>
- Chen S, Hu J, Zhuo H et al (2010) Study on the thermal-induced shape memory effect of pyridine containing supramolecular polyurethane. *Polymer (Guildf)* 51:240–248. <https://doi.org/10.1016/j.polymer.2009.11.034>
- Choi JT, Dao TD, Oh KM et al (2012) Shape memory polyurethane nanocomposites with functionalized graphene. *Smart Mater Struct* 21:75017. <https://doi.org/10.1088/0964-1726/21/7/075017>
- Domingues RMA, Gomes ME, Reis RL (2014) The potential of cellulose nanocrystals in tissue engineering strategies. *Biomacromolecules* 15:2327–2346. <https://doi.org/10.1021/bm500524s>
- Du H, Liu W, Zhang M et al (2019) Cellulose nanocrystals and cellulose nanofibrils based hydrogels for biomedical applications. *Carbohydr Polym* 209:130–144. <https://doi.org/10.1016/j.carbpol.2019.01.020>
- Du W, Zhang Z, Yin C et al (2021) Preparation of shape memory polyurethane/modified cellulose nanocrystals composites with balanced comprehensive performances. *Polym Adv Technol* 32:4710–4720. <https://doi.org/10.1002/pat.5464>
- Fortunati E, Luzi F, Janke A et al (2017) Reinforcement effect of cellulose nanocrystals in thermoplastic polyurethane matrices characterized by different soft/hard segment ratio. *Polym Eng Sci* 57:521–530. <https://doi.org/10.1002/pen.24532>
- Gao Y, Liu W, Zhu S (2018) Reversible shape memory polymer from semicrystalline poly(ethylene-co-vinyl acetate) with dynamic covalent polymer networks. *Macromolecules* 51:8956–8963. <https://doi.org/10.1021/acs.macromol.8b01724>
- Garle A, Kong S, Ojha U, Budhlall BM (2012) Thermoresponsive semicrystalline poly( $\epsilon$ -caprolactone) networks: exploiting cross-linking with cinnamoyl moieties to design polymers with tunable shape memory. *ACS Appl Mater Interfaces* 4:645
- George J, Sabapathi SN (2015) Cellulose nanocrystals: synthesis, functional properties, and applications. *Nanotechnol Sci Appl* 8:45–54. <https://doi.org/10.2147/NSA.S64386>
- Goodarzi K, Rao SS (2021) Hyaluronic acid-based hydrogels to study cancer cell behaviors. *J Mater Chem B* 9:6103–6115. <https://doi.org/10.1039/D1TB00963J>
- Goodarzi K, Jonidi Shariatzadeh F, Solouk A et al (2020) Injectable drug loaded gelatin based scaffolds as minimally invasive approach for drug delivery system: CNC/PAMAM nanoparticles. *Eur Polym J* 139:109992. <https://doi.org/10.1016/j.eurpolymj.2020.109992>
- Gupta A, Mekonnen TH (2022) Cellulose nanocrystals enabled sustainable polycaprolactone based shape memory polyurethane bionanocomposites. *J Colloid Interface Sci* 611:726–738. <https://doi.org/10.1016/j.jcis.2021.11.174>
- Ha Y, Kim Y-O, Ahn S et al (2019) Robust and stretchable self-healing polyurethane based on polycarbonate diol with different soft-segment molecular weight for flexible devices. *Eur Polym J* 118:36–44. <https://doi.org/10.1016/j.eurpolymj.2019.05.031>
- He W-N, Xu J-T (2012) Crystallization assisted self-assembly of semicrystalline block copolymers. *Prog Polym Sci* 37:1350–1400. <https://doi.org/10.1016/j.progpolymsci.2012.05.002>
- Hoidy WH, Al-Mulla EAJ, Al-Janabi KW (2010) Mechanical and thermal properties of PLLA/PCL modified clay nanocomposites. *J Polym Environ* 18:608–616. <https://doi.org/10.1007/s10924-010-0240-x>
- Jafari S, Nourany M, Zakizadeh M et al (2020) The effect of controlled phase separation of PEG/PCL-2000 homopolymer polyols using their PCL500-PEG1000-PCL500 tri-block copolymer and CNCs in the final polyurethane hydrogels on their shape memory behavior. *Compos Commun* 19:194–202. <https://doi.org/10.1016/j.coco.2020.03.016>
- Jiang S, Ji X, An L, Jiang B (2001) Crystallization behavior of PCL in hybrid confined environment. *Polymer (Guildf)* 42:3901–3907. [https://doi.org/10.1016/S0032-3861\(00\)00565-6](https://doi.org/10.1016/S0032-3861(00)00565-6)
- Jiu H, Jiao H, Zhang L et al (2016) Graphene-crosslinked two-way reversible shape memory polyurethane nanocomposites with enhanced mechanical and electrical properties. *J Mater Sci Mater Electron* 27:10720–10728. <https://doi.org/10.1007/s10854-016-5173-2>
- Joo Y-S, Cha J-R, Gong M-S (2018) Biodegradable shape-memory polymers using polycaprolactone and isosorbide based polyurethane blends. *Mater Sci Eng C* 91:426–435. <https://doi.org/10.1016/j.msec.2018.05.063>
- Kausar A (2019) Shape memory polyurethane/graphene nanocomposites: Structures, properties, and applications. *J Plast Film Sheeting* 36:151–166. <https://doi.org/10.1177/8756087919865296>
- Khadivi P, Salami-Kalajahi M, Roghani-Mamaqani H, Lotfi Mayan Sofa R (2019) Fabrication of

- microphase-separated polyurethane/cellulose nanocrystal nanocomposites with irregular mechanical and shape memory properties. *Appl Phys A* 125:779. <https://doi.org/10.1007/s00339-019-3082-y>
- Kolesov I, Dolynchuk O, Radusch HJ (2015) Shape-memory behavior of cross-linked semi-crystalline polymers and their blends. *Express Polym Lett* 9:255–276. <https://doi.org/10.3144/expresspolymlett.2015.24>
- Kumar TP, Saravanakumar S, Sankaranarayanan K (2011) Effect of annealing on the surface and band gap alignment of CdZnS thin films. *Appl Surf Sci* 257:1923–1927. <https://doi.org/10.1016/j.apsusc.2010.09.027>
- Kumar Patel K, Purohit R (2018) Future Prospects of shape memory polymer nano-composite and epoxy based shape memory polymer—a review. *Mater Today Proc* 5:20193–20200. <https://doi.org/10.1016/j.matpr.2018.06.389>
- Lahiji RR, Xu X, Reifenberger R et al (2010) Atomic force microscopy characterization of cellulose nanocrystals. *Langmuir* 26:4480–4488. <https://doi.org/10.1021/la903111j>
- Landa M, Canales J, Fernández M et al (2014) Effect of MWCNTs and graphene on the crystallization of polyurethane based nanocomposites, analyzed via calorimetry, rheology and AFM microscopy. *Polym Test* 35:101–108. <https://doi.org/10.1016/j.polymertesting.2014.03.008>
- Li M, Guan Q, Dingemans TJ (2018) High-temperature shape memory behavior of semicrystalline polyamide thermosets. *ACS Appl Mater Interfaces* 10:19106–19115. <https://doi.org/10.1021/acsami.8b03658>
- Liu Y, Li Y, Yang G et al (2015) Multi-stimulus-responsive shape-memory polymer nanocomposite network cross-linked by cellulose nanocrystals. *ACS Appl Mater Interfaces*. <https://doi.org/10.1021/am5081056>
- Lu P, Hsieh Y-L (2010) Preparation and properties of cellulose nanocrystals: rods, spheres, and network. *Carbohydr Polym* 82:329–336. <https://doi.org/10.1016/j.carbpol.2010.04.073>
- Luyt AS, Gasmí S (2016) Influence of blending and blend morphology on the thermal properties and crystallization behaviour of PLA and PCL in PLA/PCL blends. *J Mater Sci* 51:4670–4681. <https://doi.org/10.1007/s10853-016-9784-z>
- Mariano M, El Kissi N, Dufresne A (2014) Cellulose nanocrystals and related nanocomposites: review of some properties and challenges. *J Polym Sci Part B Polym Phys* 52:791–806. <https://doi.org/10.1002/polb.23490>
- Mi H-Y, Jing X, Yilmaz G et al (2018) In situ synthesis of polyurethane scaffolds with tunable properties by controlled crosslinking of tri-block copolymer and polycaprolactone triol for tissue regeneration. *Chem Eng J* 348:786–798. <https://doi.org/10.1016/j.cej.2018.04.198>
- Mu R, Hong X, Ni Y et al (2019) Recent trends and applications of cellulose nanocrystals in food industry. *Trends Food Sci Technol* 93:136–144. <https://doi.org/10.1016/j.tifs.2019.09.013>
- Müller AJ, Balsamo V, Arnal ML et al (2002) Homogeneous nucleation and fractionated crystallization in block copolymers. *Macromolecules* 35:3048–3058. <https://doi.org/10.1021/ma012026w>
- Nessi V, Falourd X, Maigret J-E et al (2019) Cellulose nanocrystals-starch nanocomposites produced by extrusion: structure and behavior in physiological conditions. *Carbohydr Polym* 225:115123. <https://doi.org/10.1016/j.carbpol.2019.115123>
- Nojima S, Yamamoto S, Ashida T (1995) Crystallization of block copolymers IV. Molecular weight dependence of the morphology formed in  $\epsilon$ -caprolactone-butadiene diblock copolymers. *Polym J* 27:673–682. <https://doi.org/10.1295/polymj.27.673>
- Noormohammadi F, Nourany M, Mir Mohamad Sadeghi G et al (2021b) The role of cellulose nanowhiskers in controlling phase segregation, crystallization and thermal stimuli responsiveness in PCL-PEGx-PCL block copolymer-based PU for human tissue engineering applications. *Carbohydr Polym* 252:117219. <https://doi.org/10.1016/j.carbpol.2020.117219>
- Nourany M, Ghelichkhani S, Sarkhosh H et al (2021) The effect of PCL/PEG ABA block lengths on the crystallization of homo/block-based polyurethane/CNW nanocomposites. *J Polym Res*. <https://doi.org/10.1007/s10965-020-02376-y>
- Park SH, Oh KW, Kim SH (2013) Reinforcement effect of cellulose nanowhisker on bio-based polyurethane. *Compos Sci Technol* 86:82–88. <https://doi.org/10.1016/j.compscitech.2013.07.006>
- Parnell S, Min K, Cakmak M (2003) Kinetic studies of polyurethane polymerization with Raman spectroscopy. *Polymer (Guildf)* 44:5137–5144. [https://doi.org/10.1016/S0032-3861\(03\)00468-3](https://doi.org/10.1016/S0032-3861(03)00468-3)
- Pei Z, Yu Z, Li M et al (2021) Self-healing and toughness cellulose nanocrystals nanocomposite hydrogels for strain-sensitive wearable flexible sensor. *Int J Biol Macromol* 179:324–332. <https://doi.org/10.1016/j.ijbiomac.2021.03.023>
- Prataviera R, Pollet E, Bretas RES et al (2018) Nanocomposites based on renewable thermoplastic polyurethane and chemically modified cellulose nanocrystals with improved mechanical properties. *J Appl Polym Sci* 135:46736. <https://doi.org/10.1002/app.46736>
- Qu Q, He J, Da Y et al (2021) High toughness polyurethane toward artificial muscles, tuned by mixing dynamic hard domains. *Macromolecules* 54:8243–8254. <https://doi.org/10.1021/acs.macromol.1c01098>
- Ranjbar HA, Nourany M, Mollavali M et al (2021) Stimuli-responsive polyurethane bionanocomposites of poly(ethylene glycol)/poly( $\epsilon$ -caprolactone) and [poly( $\epsilon$ -caprolactone)-grafted-] cellulose nanocrystals. *Polym Adv Technol* 32:76–86. <https://doi.org/10.1002/pat.5062>
- Reid MS, Villalobos M, Cranston ED (2017) Benchmarking cellulose nanocrystals: from the laboratory to industrial production. *Langmuir* 33:1583–1598. <https://doi.org/10.1021/acs.langmuir.6b03765>
- Roman M, Dong S, Hirani A, Lee YW (2009) Cellulose nanocrystals for drug delivery. In: Edgar KJ, Heinze T, Buchanan CM (eds) *Polysaccharide materials: performance by design*. American Chemical Society, Washington, DC, pp 4–81
- Rueda L, Saralegui A, Fernández d'Arlas B et al (2013) Cellulose nanocrystals/polyurethane nanocomposites. Study from the viewpoint of microphase separated structure. *Carbohydr Polym* 92:751–757. <https://doi.org/10.1016/j.carbpol.2012.09.093>

- SaifulAzry SOA, Chuah TG, Paridah MT et al (2021) Influence of cellulose II polymorph nanowhiskers on bio-based nanocomposite film from *Jatropha* oil polyurethane. *Mater Res Express* 8:15003. <https://doi.org/10.1088/2053-1591/abc6ce>
- Saralegi A, Fernandes SCM, Alonso-Varona A et al (2013) Shape-memory bionanocomposites based on chitin nanocrystals and thermoplastic polyurethane with a highly crystalline soft segment. *Biomacromol* 14:4475–4482. <https://doi.org/10.1021/bm401385c>
- Sarkhosh H, Nourany M, Noormohammadi F et al (2021) Development of a semi-crystalline hybrid polyurethane nanocomposites for hMSCs cell culture and evaluation of body-temperature shape memory performance and isothermal crystallization kinetics. *J Polym Res*. <https://doi.org/10.1007/s10965-021-02522-0>
- Scetta G, Ju J, Selles N et al (2021) Strain induced strengthening of soft thermoplastic polyurethanes under cyclic deformation. *J Polym Sci* 59:685–696. <https://doi.org/10.1002/pol.20210060>
- Shirole A, Nicharat A, Perotto CU, Weder C (2018) Tailoring the properties of a shape-memory polyurethane via nanocomposite formation and nucleation. *Macromolecules* 51:1841–1849. <https://doi.org/10.1021/acs.macromol.7b01728>
- Striebeck N, Li X, Kogut I et al (2015) Morphological failure mechanisms in tensile tests of crosslinked polyurethanes with poorly developed domain structure. *Macromol Mater Eng* 300:699–711. <https://doi.org/10.1002/mame.20150007>
- Tang J, Sisler J, Grishkewich N, Tam KC (2017) Functionalization of cellulose nanocrystals for advanced applications. *J Colloid Interface Sci* 494:397–409. <https://doi.org/10.1016/j.jcis.2017.01.077>
- Tian D, Wang F, Yang Z et al (2019) High-performance polyurethane nanocomposites based on UPy-modified cellulose nanocrystals. *Carbohydr Polym* 219:191–200. <https://doi.org/10.1016/j.carbpol.2019.05.029>
- Tingaut P, Zimmermann T, Sèbe G (2012) Cellulose nanocrystals and microfibrillated cellulose as building blocks for the design of hierarchical functional materials. *J Mater Chem* 22:20105–20111. <https://doi.org/10.1039/C2JM32956E>
- Tito NB, Creton C, Storm C, Ellenbroek WG (2019) Harnessing entropy to enhance toughness in reversibly crosslinked polymer networks. *Soft Matter* 15:2190–2203. <https://doi.org/10.1039/C8SM02577K>
- Trache D, Hussin MH, Haafiz MKM, Thakur VK (2017) Recent progress in cellulose nanocrystals: sources and production. *Nanoscale* 9:1763–1786. <https://doi.org/10.1039/C6NR09494E>
- Urbina L, Alonso-Varona A, Saralegi A et al (2019) Hybrid and biocompatible cellulose/polyurethane nanocomposites with water-activated shape memory properties. *Carbohydr Polym* 216:86–96. <https://doi.org/10.1016/j.carbpol.2019.04.010>
- Vanderfleet OM, Cranston ED (2021) Production routes to tailor the performance of cellulose nanocrystals. *Nat Rev Mater* 6:124–144. <https://doi.org/10.1038/s41578-020-00239-y>
- Vilgis T, Halperin A (1991) Aggregation of coil-crystalline block copolymers: equilibrium crystallization. *Macromolecules* 24:2090–2095. <https://doi.org/10.1021/ma00008a058>
- Vorov OK, Livesay DR, Jacobs DJ (2008) Conformational entropy of an ideal cross-linking polymer chain. *Entropy*. <https://doi.org/10.3390/e10030285>
- Wang Y-J, Jeng U-S, Hsu S (2018a) Biodegradable water-based polyurethane shape memory elastomers for bone tissue engineering. *ACS Biomater Sci Eng* 4:1397–1406. <https://doi.org/10.1021/acsbiomaterials.8b00091>
- Wang Y, Cheng Z, Liu Z et al (2018b) Cellulose nanofibers/polyurethane shape memory composites with fast water-responsivity. *J Mater Chem B* 6:1668–1677. <https://doi.org/10.1039/C7TB03069J>
- Wu XL, Kang SF, Xu XJ et al (2014) Effect of the crosslinking density and programming temperature on the shape fixity and shape recovery in epoxy–anhydride shape-memory polymers. *J Appl Polym Sci*. <https://doi.org/10.1002/app.40559>
- Wu H, Xie H, Tian X et al (2021) Hard, tough and fast self-healing thermoplastic polyurethane. *Prog Org Coat* 159:106409. <https://doi.org/10.1016/j.porgcoat.2021.106409>
- Xiang N, Zhang X, Zheng M et al (2021) Investigation of tensile behavior and molecular structure of the thermoplastic polyurethane sheets injection molded at different mold temperatures. *J Appl Polym Sci* 138:50959. <https://doi.org/10.1002/app.50959>
- Xie H, Du H, Yang X, Si C (2018) Recent strategies in preparation of cellulose nanocrystals and cellulose nanofibrils derived from raw cellulose materials. *Int J Polym Sci* 2018:7923068. <https://doi.org/10.1155/2018/7923068>
- Yu K, Ge Q, Qi HJ (2014) Reduced time as a unified parameter determining fixity and free recovery of shape memory polymers. *Nat Commun* 5:1–9. <https://doi.org/10.1038/ncomms4066>
- Zakizadeh M, Nourany M, Javadzadeh M et al (2021) Analysis of crystallization kinetics and shape memory performance of peg-pcl/mwcnt based pu nanocomposite for tissue engineering applications. *Express Polym Lett* 15:418–432. <https://doi.org/10.3144/expresspolymlett.2021.36>
- Zare M, Prabhakaran MP, Parvin N, Ramakrishna S (2019) Thermally-induced two-way shape memory polymers: mechanisms, structures, and applications. *Chem Eng J* 374:706–720. <https://doi.org/10.1016/j.cej.2019.05.167>
- Zeng H, Sun H, Gu J (2021) Modeling the one-way and two-way shape memory effects of semi-crystalline polymers. *Smart Mater Struct* 30:95020. <https://doi.org/10.1088/1361-665x/ac179e>
- Zhang K, Zhao Z, Huang J et al (2019a) Self-recoverable semi-crystalline hydrogels with thermomechanics and shape memory performance. *Sci China Mater* 62:586–596. <https://doi.org/10.1007/s40843-018-9347-5>
- Zhang Y, Hu J, Zhao X et al (2019b) Mechanically robust shape memory polyurethane nanocomposites for minimally invasive bone repair. *ACS Appl Bio Mater* 2:1056–1065. <https://doi.org/10.1021/acsabm.8b00655>
- Zhou J, Turner SA, Brosnan SM et al (2014) Shapeshifting: reversible shape memory in semicrystalline elastomers.

Macromolecules 47:1768–1776. <https://doi.org/10.1021/ma4023185>

Zhuravlev E, Schmelzer JWP, Wunderlich B, Schick C (2011) Kinetics of nucleation and crystallization in poly( $\epsilon$ -caprolactone) (PCL). *Polymer (Guildf)* 52:1983–1997. <https://doi.org/10.1016/j.polymer.2011.03.013>

Springer Nature or its licensor holds exclusive rights to this article under a publishing agreement with the author(s) or other rightsholder(s); author self-archiving of the accepted manuscript version of this article is solely governed by the terms of such publishing agreement and applicable law.

**Publisher's Note** Springer Nature remains neutral with regard to jurisdictional claims in published maps and institutional affiliations.